Bioelectric Modulation of Membrane Potential in Human Adipose-Derived Stem Cells

An Honors Thesis for the Department of Biology

Sophia Bunnell

Kaplan Lab

Tufts University, 2018

Table of Contents

List of Tables

List of Figures

Abstract

The role of membrane potential in adipose-derived stem cell (ASC) patterning has yet to be elucidated. To assess the effects of membrane potential modulation on human ASC behavior, ASCs were cultured in 2D treated and with membrane potential-altering drugs such as ivermectin. Additionally, to assess the combined effects of membrane potential modulation in a three-dimensional microenvironment, ASCs were also cultured on silk fibroin sponges and treated with ivermectin. While some experiments showed ivermectin induce an increase in ASC proliferation, others did not show the same effect. Future experiments can be undertaken to evaluate the modulation of membrane potential in ASCs including use of other electroceutical drugs, assessing combined effects of growth factors, and performing experiments in media with defined chloride levels.

Introduction

Adipose-Derived Stem Cells

Adipose-derived stem cells are a subset of mesenchymal stem cells (MSCs) that reside in the vascular niche of adipose tissue. While best known for their adipogenic potential, adipose-derived stem cells also possess significant osteogenic and chondrogenic potential (Johal et al., 2015). Adipose-derived stem cells have great potential for tissue engineering and regenerative medicine applications and have been the subject of much study since they were discovered in 2002 (Zuk et al., 2002).

Adipose-derived stem cells (ASCs) can be easily isolated from abdominoplasty or liposuction patient samples and yield an order of magnitude more cells than bone marrow-derived stem cell harvest (Bunnell et al., 2008). Given that ASCs can be isolated from individual patients undergoing low-risk elective procedures, they hold significant potential for autogenic transplantation and have been the focus of multiple recent clinical trials.

Phase I and II clinical trials have been performed to evaluate the safety of autologous ASC injection for numerous soft tissue defects, autoimmune diseases, cardiovascular diseases, and diabetes. Phase III trials have been performed for the treatment of fistulas secondary to Crohn's disease with positive results. ASCs have been shown to have a good safety profile in multiple clinical trials, with few adverse effects reported to date (Gir et al., 2012). A recent human pediatric case study has shown evidence for autogenic ASC transplantation aiding in bone

regeneration following severe craniofacial injury with no adverse effects (Gir et al., 2012).

ASCs are also promising therapeutic candidates due to their immunomodulatory properties. Specifically, ASCs have been shown to suppress inflammatory cytokine production and stimulate IL-10 production by mediation of T cell responses (Lindroos et al., 2011). ASCs are in the process of being investigated for their potential uses in autoimmune diseases such as ulcerative colitis, Crohn's disease, and rheumatoid arthritis (Gonzalez-Rey et al., 2010). Early mouse studies have shown promising results for ulcerative colitis, with ASC-treated mice showing diminished weight loss and inflammation and increased survival (González et al., 2009).

Adipose-derived stem cells are also known to secrete immunomodulatory factors that aid wound healing and have been shown to have a good safety profile in human clinical trials (Hassan et al., 2014). Another mechanism by which MSCs are known to aid in wound healing is through differentiation and angiogenesis (Wu et al., 2007). ASCs have been shown to increase fibroblast proliferation via paracrine factor secretion, making ASCs promising candidates for wound healing therapies (Kim et al., 2007). ASC extract has also been shown to aid cutaneous wound healing in an vivo mouse study and also increase human fibroblast proliferation in vitro, further supporting ASC's roles as paracrine factor secretors in wound healing (Na et al., 2017).

ASCs are particularly easy to isolate in culture given their strong adherence to uncoated tissue culture plastic. ASCs can be also be cryopreserved

easily, which opens up the possibility of cell banking for individuals (Zuk, 2013). Because liposuction is a minimally invasive procedure, this could be a feasible solution for cell banking for regenerative medicine in the future. Another advantage of ASC use is that the yield from an individual patient sample can be in the order of tens to hundreds of millions of cells (Iyyanki et al., 2015). Therefore, they often do not have to be expanded before use in tissue engineering applications. This is especially important because it minimizes passage number and time outside the body, which decreases the risk of genetic drift or contamination. For use in human clinical applications, it is important that expansion is xeno-free, which can be achieved with the use of human platelet lysate in the place of FBS (Escobar and Chaparro, 2016). However, the use of human-derived components can be costly. Additionally, expansion of ASCs is time consuming and requires skilled labor. Therefore, the high yield from ASC isolation reduces costs and increases potential for scalability.

To isolate ASCs, abdominoplasty samples are crudely homogenized by mincing. As liposuction samples are already homogenized, the processing procedure is the same for both abdominoplasty and liposuction samples. The samples are next digested with collagenase Type I. The digest is centrifuged, then the stromal vascular fraction is isolated and plated on tissue culture plastic. The adherent cells are the adipose-derived stem cells and can be further characterized by flow cytometry to ensure expression of ASC markers before experimentation (Bunnell et al., 2008).

Adipose-derived stem cell positive surface markers are generally accepted to include CD10, CD13, CD29, CD34, CD44, CD49e, CD59, CD73, CD90, CD105, and CD166, while negative markers are generally accepted to be CD11b, CD14, CD19, CD31, CD45, CD56, and CD146 (Mildmay-White and Khan, 2017). It is imperative to properly characterize cell surface markers upon ASC isolation to ensure that the population isolated expresses the correct markers and that fibroblasts were not mistakenly isolated.

As ASCs are primary cells and not well characterized cell lines, there is inherent patient variability between donor samples. This necessitates the use of cells from multiple donors to ensure that observed trends are representative at a population level. Additionally, ASCs are not pluripotent and cannot be differentiated into every lineage. Therefore, the applications of differentiated ASCs are limited to specific lineages.

Adipose-derived stem cells have been shown to have endodermal, ectodermal, and mesodermal differentiation capability and have been reported to differentiate into hepatic, pancreatic, and neuronal cell types in addition to adipose, cartilaginous, and bone cell types (Frese et al., 2016; Johal et al., 2015), Numerous animal studies have demonstrated ASC utility for in vivo differentiation into bone, cartilage, muscle, fat, and endothelial tissues (Tsuji et al., 2014; Zuk, 2013).

ASC differentiation into adipocytes can be initiated by the addition of isobutyl- methylxanthine, insulin, and indomethacin into the media. Mature, unilocular adipocytes are typically produced in three weeks (Choi et al., 2010). A

commonly used marker for adipogenesis is the transcription factor PPAR-γ (Tyagi et al., 2011). ASCs can also be osteogenically induced in two weeks with dexamethasone, b-glycerolphosphate, and ascorbate-2-phosphate, or chondrogenically induced in three weeks with the use of high glucose DMEM, bone morphogenic protein-6, TGF-b3, dexamethasone, ascorbate 2-phosphate, proline, pyruvate, insulin, transferrin, selenous acid, and linoleic acid (Bunnell et al., 2008).

Additionally, the three-dimensional substrates on which ASCs are grown are known to impact differentiation. Substrate stiffness has been shown to impact ASC taxis, with a specific threshold of stiffness necessary for ASCs to exhibit durotaxis up a stiffness gradient (Hadden et al., 2017). Additionally, substrates that mimic in vivo adipose tissue stiffness aid in adipogenic differentiation, while stiffer substrates promote osteogenic differentiation (Young et al., 2013; Zhang et al., 2018).

While many different growth factors and substrates have been evaluated for their impact on ASC differentiation, the role of bioelectric signaling on ASC differentiation is poorly studied. There is data that suggests membrane potential is involved with bone marrow-derived MSC differentiation into adipogenic and osteogenic lineages, with depolarization preventing differentiation and hyperpolarization promoting differentiation. Significantly, depolarization via increased K^+ in the media induced reversal of differentiation despite the presence of osteogenic or adipogenic differentiation factors (Sundelacruz et al., 2008). This indicates that membrane potential's role in cell fate may overrule that of growth

factors. However, there is still much to discover about the effects of membrane potential on ASC behavior that is not well studied.

While the impacts of membrane potential have been studied extensively in excitable cells types such as neurons and cardiomyocytes, basic science knowledge of the role of membrane potential in non-excitable cell types is less well characterized. To gain insight on the overarching developmental pathways influenced by membrane potential, it is essential to allocate significant resources to understanding bioelectric signaling in stem cells.

Bioelectricity and Membrane Potential

Bioelectricity describes the electrical potentials and currents found in living systems and is performed via ion channels, pumps, and gap junctions found in the cell membrane. Specifically, bioelectric signaling has been shown to be implicated in numerous developmental processes including embryonic development, cellular differentiation, and left-right asymmetry. Bioelectric signals have also been implicated in cell patterning and migration (Levin, 2014). Taken together, bioelectric processes provide a potential explanation for the coordination of developmental processes at an organismal level.

Membrane potential (V_{mem}) arises from the differences in ionic concentrations on the intracellular and extracellular sides of an individual cell's plasma membrane. The difference in ionic concentrations generates a voltage across the membrane, which is known as the membrane potential. Resting membrane potential refers to the typical membrane potential when an action

potential or other such activity is not occurring. In non-excitable cells, the resting membrane potential is generally the parameter that is recorded and studied.

It is necessary to actively maintain ionic gradients in the cell, even in a resting state, as intracellular potassium concentration is much higher than extracellular concentration and intracellular sodium concentration is much lower than extracellular concentration. One of the major active mechanisms used to maintain these gradients is the action of ATPase pumps. ATPase pumps energetically couple the hydrolysis of ATP to the transport of specific small molecules against their concentration gradients. One of the most highly energetically expensive processes a cell performs is the use of Na^+/K^+ ATPase pump, which maintains appropriate ionic concentrations by pumping Na^+ outward and K^+ inward (Lodish et al., 2000).

Ions are also transported passively down their concentration gradients. The two main types of proteins through which ions move passively are pores and channels. Pores typically do not display specific ion selectivity, while channels often do display selectivity. Ion channels are often gated and thus require a specific stimulus to either open or close. Ion channels can be voltage-gated, mechanically gated, ligand-gated, neurotransmitter-gated, ion-gated, or nucleotide-gated (Alberts et al., 2002; Lodish et al., 2000). K^+ leak channels, which are always open, are an example of non-gated ion channels (Alberts et al., 2002). Additionally, a small component of membrane potential arises through direct diffusion of ions across the plasma membrane, although the membrane is only very slightly permeable to ions.

Membrane potential is not static across the life of a cell and can be altered due to changes ion channel expression and by the activation or inactivation of specific ion channels. Membrane potential has also been shown to vary with the phase of the cell cycle (Blackiston et al., 2009; Sachs et al., 1974). Cells with greater stem cell or proliferative character typically have more depolarized resting membrane potentials (Figure 1). Conversely, more terminally differentiated cells tend to have more hyperpolarized resting membrane potentials (Levin et al., 2017).

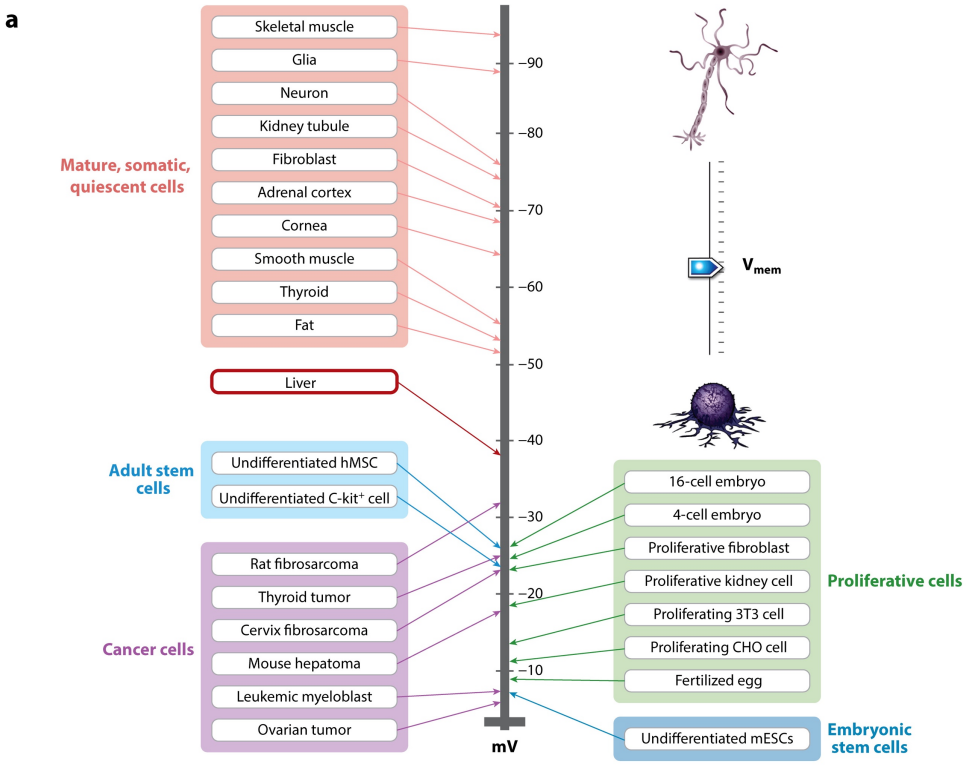

Figure 1. Resting membrane potentials of more proliferative cell types tend to be more depolarized (Levin et al., 2017).

The impact of membrane potential on cell behavior has recently been a topic of much study due to observed changes in cell patterning and functional response. Specifically, membrane potential modulation has been shown to alter cell proliferation in neonatal cardiomyocytes in vitro (Lan et al., 2014). Membrane potential modulation has also been shown to alter neuron arrangement and connectivity in vitro (Özkucur et al., 2015). Bioelectricity has also been implicated in overarching developmental patterning, such as in *Xenopus laevis* embryonic eye patterning (Pai et al., 2012). These bioelectric signals are transduced by a broad variety of cell signaling systems

Specifically, bioelectric signals are known to be transduced by multiple diverse mechanisms, including small molecule signaling, serotonin signaling, butyrate signaling, and PTEN phosphatase signaling (Figure 2, Levin et al., 2017). Small molecule signaling includes Ca^{2+} signaling, which is known to play a role in numerous signaling cascades. Membrane potential has also been shown to regulate transcription of the K^+ leak channel TASK-3, also known as KCNK9, via the calcineurin pathway when Ca^{2+} influx was induced by depolarizing culture conditions (Zanzouri et al., 2006).

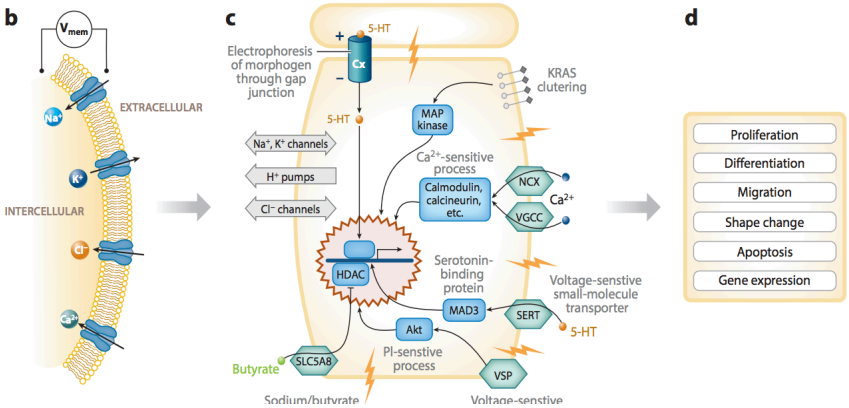

Figure 2. An overview of bioelectric signal transduction pathways shows the breadth of bioelectric signaling in the cell (Levin et al., 2017).

Measurement of Membrane Potential

There are direct and indirect methods for membrane potential measurement. A commonly employed direct technique is whole cell patch clamping. In this technique, a glass pipette is filled with solution that mimics extracellular solution and used to form a seal with the cell membrane. Suction is then applied to rupture the membrane, giving the pipette intracellular access. The pipette has an electrode inside it that allows for the measurement of voltage, current, and capacitance (Zhao et al., 2009).

Fluorescent bioelectricity reporter dyes can also be utilized to measure membrane potential indirectly. There are two general categories of fluorescent reporter dyes: slow-response and fast response. Slow response dyes typically work by diffusing across the cell membrane, which alters fluorescence signal. Fast response dyes typically alter their fluorescence in response to a conformational change induced by intramolecular charge distribution (Miller, 2016). Voltage reporter dyes are advantageous because they can be used to study populations of cells, bioelectric gradients, and measure membrane potential over time. Desirable characteristics for dyes include resistance to photobleaching and low toxicity to the cell so that time-resolved live imaging can be performed. It can be difficult to accurately quantify membrane potential with the use of voltage dyes, so data is often reported as fold change rather than absolute membrane potential values.

Differentiation and Membrane Potential

Transcriptional responses downstream of resting membrane potential change have been shown to be evolutionarily conserved across *Xenopus*, Axolotl, and human MSCs, suggesting that membrane potential related pathways serve an overarching role in development (Levin et al., 2017). To study membrane potential, reliable methods for alteration of membrane potential in the laboratory are necessary. Membrane potential can be experimentally altered with ionophores, ionic drugs which change extracellular ionic concentration, and channel-opening or blocking drugs. To modify extracellular ionic concentration, potassium gluconate is often used as a source of extracellular potassium without providing a chloride counter-ion. Another often used drug is ivermectin, which is known to bind the mammalian chloride channel GlyR (Chen and Kubo, 2017).

Ivermectin

Ivermectin has high affinity for invertebrate glutamate-gated chloride channels, which are similar in structure to mammalian glycine receptors. Ivermectin activates these channels, causing an influx of chloride (Wolstenholme and Rogers, 2005; Wolstenholme, 2011, 2012; Meyers et al., 2015). This action is highly effective at killing invertebrate parasites, and consequentially ivermectin is widely used for the treatment of nematode, louse, and mite infections (Crump and Omura, 2011).

Ivermectin has several well-characterized mammalian targets. Some of the most well-studied mammalian targets include GlyR, a neuronally expressed channel; P2X4, an ATP-gated purinergic channel; GIRK, a K^+ inward rectifying current channel; and FXR, the nuclear farnesoid X receptor which regulates triglyceride and glucose metabolism in the liver (Chen and Kubo, 2017; Table 1). Via these targets, ivermectin has been shown to alter cell behavior in culture. Ivermectin has been of specific interest in hyperpolarization-dependent treatment of leukemia, as it was shown to preferentially kill leukemia cells while sparing healthy cells in a mouse model (Sharmeen et al., 2010). Additionally, ivermectin has been shown to affect cell proliferation by altering the polymerization dynamics of tubulin (Ashraf and Prichard, 2016). Therefore, ivermectin can affect a diverse array of cellular machinery and broadly impact cell behavior.

Table 1. Mammalian Targets for Ivermectin (Adapted from Chen and Kubo, 2017)

Target Protein	**Function**	**EC_{50}**
GlyR	Cl^- inward	1-5μM
P2X4	Ca^{2+} inward	0.25μM
GIRK	K^+ inward	3.5-7.5μM
FXR	Transcriptional regulation of triglyceride/glucose metabolism	0.2μM

Biomaterials

To examine ASC behavior in response to membrane potential modulation, it is essential to study the cells in a three-dimensional (3D) microenvironment to recapitulate a more physiologically relevant environment. 3D culture has several advantages over 2D culture, including the capacity to support a greater number of cells and allow better cell-extracellular matrix interaction (McKee and Chaudhry,

2017). Many biomaterials have been used for 3D culture, including silk, collagen, hyaluronic acid, and alginate (Dhaliwal, 2018).

Collagen scaffolds are advantageous due to their biocompatibility, high porosity, and incorporation into the tissue-engineered construct. However, collagen has the potential for antigenicity if telopeptides are not first removed by proteolysis (Glowacki and Mizuno, 2008). Hyaluronic acid is a glycosaminoglycan that can be used to fabricate tunable, bioabsorbable scaffolds. However, these scaffolds have poor mechanical properties if they are not crosslinked. Crosslinking compounds are often highly toxic, so care must be taken to fully remove them (Collins and Birkinshaw, 2013). Alginate is a polymer derived from brown seaweed that is often to make RGD-functionalized scaffolds which promote cell adhesion. However, alginate scaffolds can experience significant variability due to the inherent nature of seaweed harvest. Additionally, alginate is poorly degraded by the body (Lee and Mooney, 2012).

Silk fibroin is an excellent biomaterial for the growth of three-dimensional (3D) in vitro cultures. Silk properties are highly tunable and degradation rate can be controlled such that it can be adapted to degrade over weeks to months. It is also non-toxic upon degradation and non-immunogenic (Lee and Mooney, 2012). Silk fibroin can be used to prepare a wide variety of biomaterials, including silk films, hydrogels, and sponges (Vepari and Kaplan, 2007). Each material is suited to specific applications, making silk fibroin a versatile and useful material. Silk is especially biocompatible and widespread in vivo data is available to support its use (Thurber et al., 2015).

Silk fibroin sponges have been previously used to culture and differentiate ASCs successfully (Choi et al., 2011). Additionally, silk scaffolds have been shown to support long term in vitro cultures of white adipose, cortical brain, intestine, kidney, and bone tissue (Abbott et al., 2016). Therefore, silk fibroin sponges are an ideal biomaterial for the recapitulation of a 3D environment when culturing ASCs.

In this study, we aimed to assess the effects of bioelectric signaling on ASC behavior. To do so, we cultured donor-derived ASCs in the presence of multiple membrane potential-altering drugs. Experiments were performed in both 2D and 3D culture to evaluate cell response in different microenvironments. Functional behaviors such as cell migration and proliferation, cytokine release, and membrane potential were assessed to determine the impacts of bioelectric signaling.

Methods

Cell Culture

Adipose-derived stem cells were purchased from Lonza. Briefly, cells were thawed and seeded at 5000 cells/cm^2 density. Cells were grown and expanded in DMEM/F12 containing 10% fetal bovine serum, 1% antibiotic-antimycotic (Gibco), 5ng/mL EGF, 1ng/mL bFGF and 0.25ng/mL TGF-B (R&D Systems). EGF, bFGF and TGF-B were used for cell expansion only and withdrawn upon experimentation. Media was changed every 72 hours. Cells were cultured in a humidified cell culture incubator at 37°C with 5% CO^2 and passaged at 90% confluence. Cells were used for experimentation were between P2-P6.

Preparation of Ivermectin and Potassium Gluconate

To prepare ivermectin stock, ivermectin powder (Sigma, molecular weight =875.1g/mol) was dissolved in DMSO for a stock concentration of 5mM and stored at 4°C. To prepare ivermectin for cell culture use, the 5mM stock was first diluted 1:100 in cell culture media for a concentration of 50μM to avoid pipetting small volumes before further dilution in cell culture media to 0.1-1.0μM working concentration.

To prepare potassium gluconate stock, powder (Sigma, molecular weight =234.2g/mol) was dissolved in deionized water and 0.2μM filter sterilized for a

stock concentration of 1M and stored at 4°C. To prepare working concentration solution (40-80mM), the 1M stock was directly diluted in cell culture media.

Scratch Assay

Cells were seeded at 15,000 cells/cm^2 in a 24 well plate 24 hours before experimentation. After 24 hours a P200 pipette tip was used to make a straight scratch down the center of each well as described in (Liang et al., 2007). Time lapse imaging was performed every thirty minutes for forty hours. Scratch area was determined using the image analysis software CellProfiler (Carpenter et al., 2006). A representative image shows one cycle of time lapse image analysis (Figure 3).

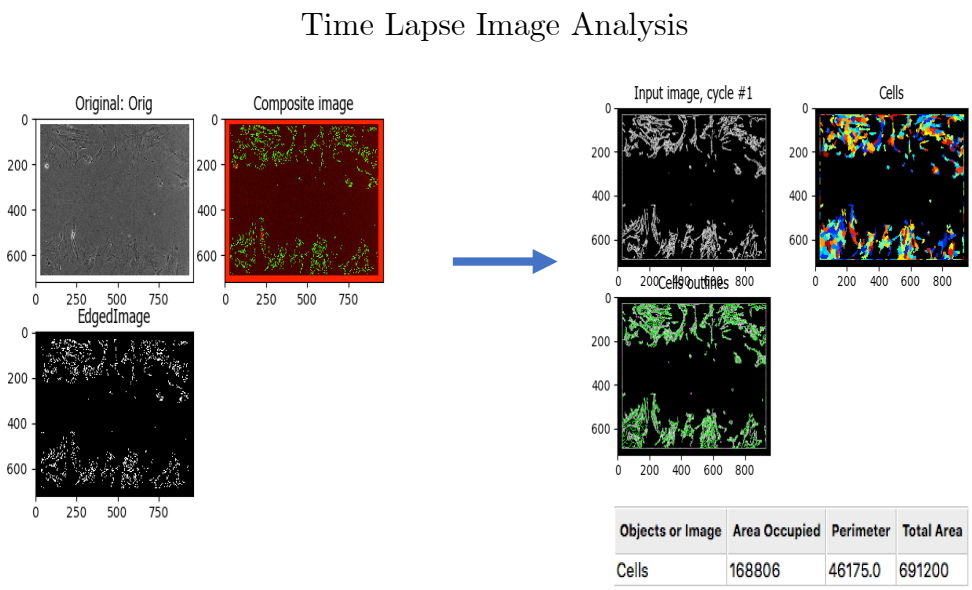

Figure 3. A representative image of CellProfiler's scratch assay pipeline in progress for time lapse image analysis.

Silk Scaffold Preparation

Bombyx mori cocoons were chopped and the inner worm was removed. Cocoon pieces were then boiled for 30 minutes in 0.02M Na_2CO_3 and rinsed to remove sericin, leaving silk fibroin. Fibroin was then solubilized in 9M LiBr before dialysis against water to obtain 6% weight/volume silk fibroin solution. Twenty grams of 500-600µm size granular NaCl was added to 10mL silk fibroin solution in a petri dishes and incubated at room temperature for 24 hours. Scaffolds were then soaked in water for two days with several water changes to remove the granular NaCl. The resulting sponge was punched out with a 6mm diameter biopsy punch and scaffolds were trimmed to 2mm thickness. Scaffolds were autoclaved before use in cell culture.

3D Cell Culture

Silk fibroin scaffolds were coated laminin in PBS for one hour at 37°C, then rinsed with ASC media. Cells were seeded at 500,000 cells in 50µL volume and allowed to attach to scaffolds for one hour before 450µL additional media was added to the well. Scaffolds were incubated at 37°C in a humidified incubator with 5% CO_2. Media was changed every 48 hours.

For the 3D migration and proliferation assay, cells were densely seeded on two 6mm silk fibroin sponges and grown for 48 hours. A third, empty scaffold was then abutted between the two seeded scaffolds after 48 hours and secured. After two to ten days, cell number was measured by Picogreen in both the outer and inner scaffolds.

WST-1 and Picogreen

The WST-1 assay was used to measure cell metabolic activity. 2D cell cultures were incubated for one hour with the WST-1 reagent diluted 1:10 in cell culture medium (Roche). Optical density was then measured at 420 nm using a microplate reader. The Picogreen Quant-iT assay was used as a measure of DNA content and therefore overall cell number (ThermoFisher). Cells were lysed in 0.02% Triton-X100 in PBS and stored at -20°C. To perform the assay, lysate thawed then further diluted in TE buffer. A standard curve was generated using λ phage DNA of known concentration. Picogreen reagent was added at 1:200 concentration and samples were incubated for four minutes before reading fluorescence at 485/538nm in a microplate reader. WST-1 and Picogreen data was statistically analyzed with ANOVA followed by Bonferroni correction with the significance level set to 0.05.

Membrane Potential Measurement using Voltage Reporter Dyes

2D cell cultures were incubated with either 200nM SS44 di-anionic (Levin Lab, Akita Innovations) for one hour, or 0.475μM $DiBAC_4(3)$ for one hour, 10μM $DiSBAC_2(3)$ for one hour, or 2μM Di-8-ANEPPS (ThermoFisher) for 30 minutes in cell culture media at 37°C. For SS44 (di-anionic) and Di-8-ANEPPS, cultures were then gently washed twice with PBS before imaging, while $DiBAC_4(3)$ and $DiSBAC_2(3)$ samples were imaged without washing.

Membrane Potential Measurement using Whole-Cell Patch Clamping

ASCs were seeded at 5,000 cells/cm2 in a 35mm dish and cultured with and without 0.1μM ivermectin for three hours to five days. Immediately before patch clamp measurement, cells were trypsinized for 15 seconds to round cells without detaching them. Cells were then allowed to recover at 37°C for five minutes before measurement. Media was then aspirated and replaced with extracellular solution. For ivermectin-treated conditions, the extracellular solution also contained ivermectin. Patch pipettes were filled with intracellular solution, then membrane potential was measured at room temperature using whole cell patch clamp in current clamp mode.

Results

Metabolic Activity Changes in Response to V_{mem}-Altering Drugs

To experimentally alter ASC membrane potential, four drugs were selected for their known abilities to alter membrane potential in other cell types: pinacidil, glibenclamide, potassium gluconate, and ivermectin. To evaluate the toxicity of membrane potential altering drugs on ASCs, WST-1 was used as an indicator of cell metabolism. Cells were grown for 24, 48, and 72 hours in the presence of multiple concentrations of V_{mem}-altering drugs. Both pinacidil and glibenclamide were found to decrease cell metabolic activity at 72 hours at all concentrations tested except for 0.4µM pinacidil (Figure 4). Ivermectin was not found to change metabolic activity, while potassium gluconate was found to increase metabolic activity at 24 hours at 40, 60 and 80mM concentration, and at 48 hours at 60mM and 80mM concentration. At 72 hours, 80mM potassium

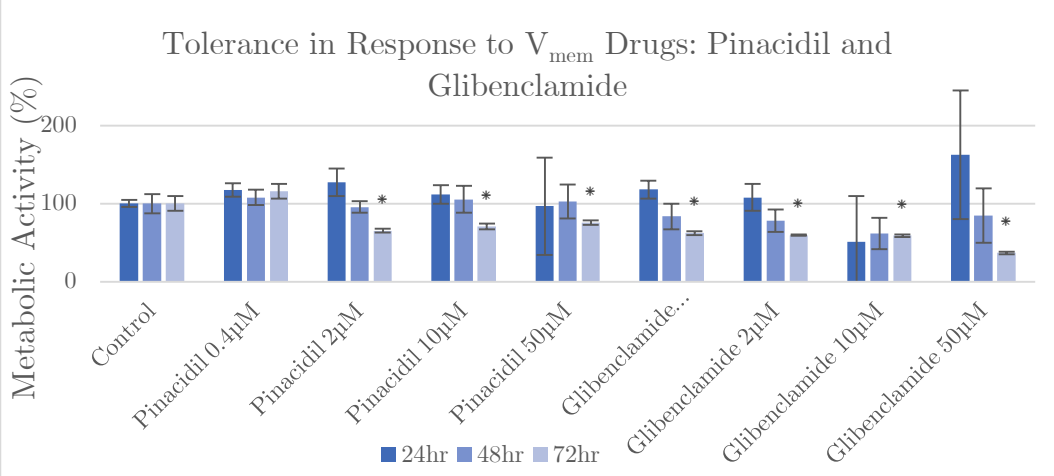

Figure 4. WST-1 measurement for pinacidil and glibenclamide. No drug treatments significantly differed from the control at 24 and 48 hours, while all drug treatments except 0.4µM pinacidil caused significant decreases in cell metabolic activity at 72 hours (ANOVA, n=6).

gluconate treatment was found to significantly decrease metabolic activity (Figure 5).

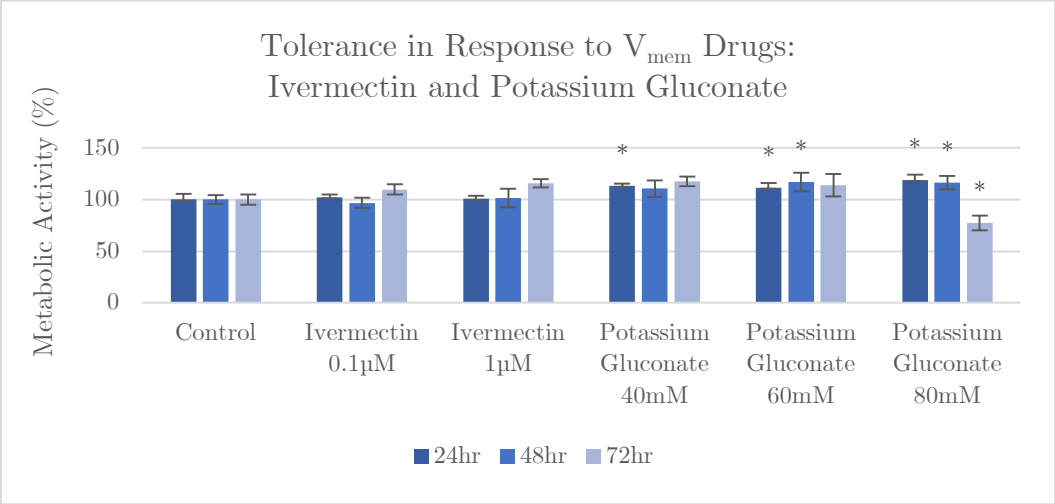

Figure 5. WST-1 measurement for potassium gluconate and ivermectin. Ivermectin treatment was not found to alter metabolic activity, while potassium gluconate was found to significantly increase metabolic activity for several treatments and significantly decrease metabolic activity at 80mM concentration by 72 hours (ANOVA, n=6).

Ivermectin

Cell proliferation is an important metric of cell behavior. To determine if ivermectin treatment alters ASC proliferation in 2D, cells were seeded in 2D and grown in the presence of multiple concentrations of ivermectin for up to two weeks. To assess potentially donor-specific ASC responses, cells from multiple donors were compared. Donor to donor variability was observed for ivermectin tolerance in 2D (Figures 6, 7, 8). For Donor 2, no differences between the control and 0.1μM ivermectin treatment were observed for any time points (Figure 6). For Donor 3, significant decreases in cell number were observed at 48 hours for 0.5μM and 1.0μM ivermectin concentration, while 0.1μM concentration did not show any significant difference from the control (Figure 7). For Donor 4, only 1.0μM ivermectin at 48 hours was found to significantly increase cell number relative to the control (Figure 8).

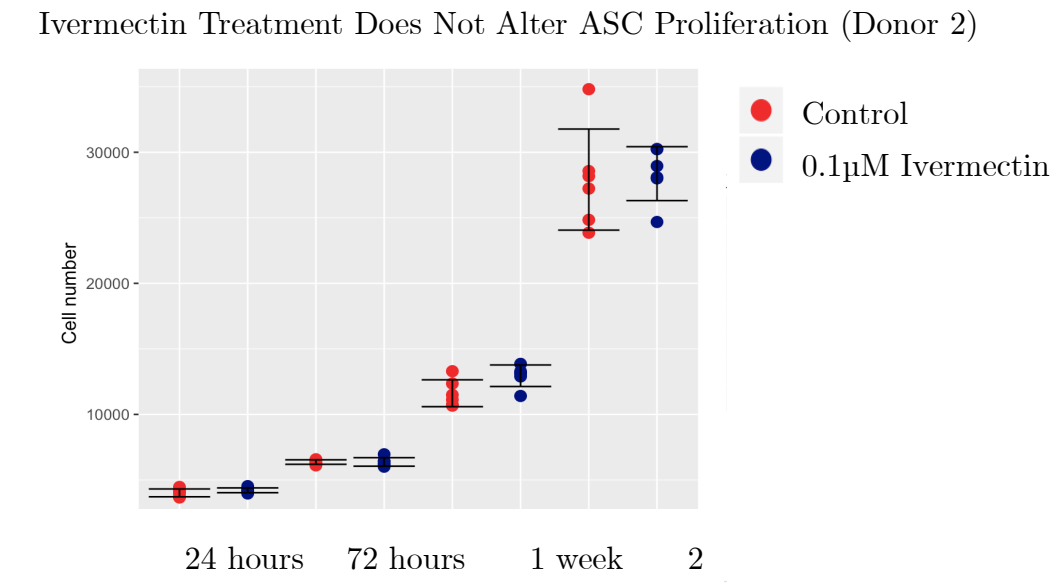

Figure 6. 2D Ivermectin Tolerance for Donor 2. ASCs treated with 0.1µM ivermectin show no significant change in proliferation at any timepoint. Cell number was measured with Picogreen. Error bars represent standard deviation (ANOVA, $p > 0.05$, n=6 per treatment).

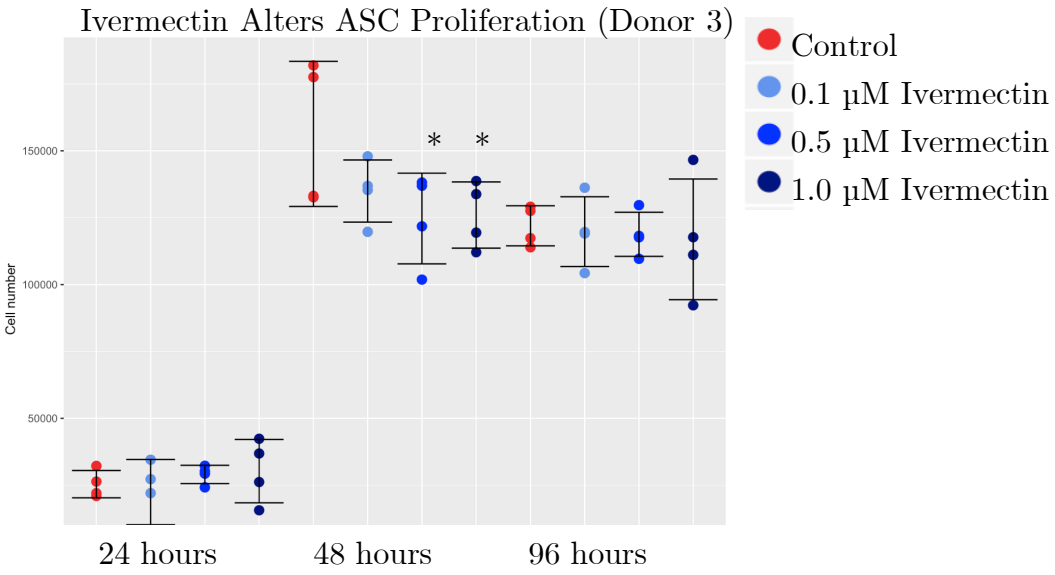

Figure 7. 2D Ivermectin Tolerance for Donor 3. A significant decrease in cell number was observed at 48 hours between the control and ASCs treated with 0.5µM and 1.0µM ivermectin. Cell number was measured with Picogreen. Error bars represent standard deviation (ANOVA, $p < 0.05$, n=4 per treatment).

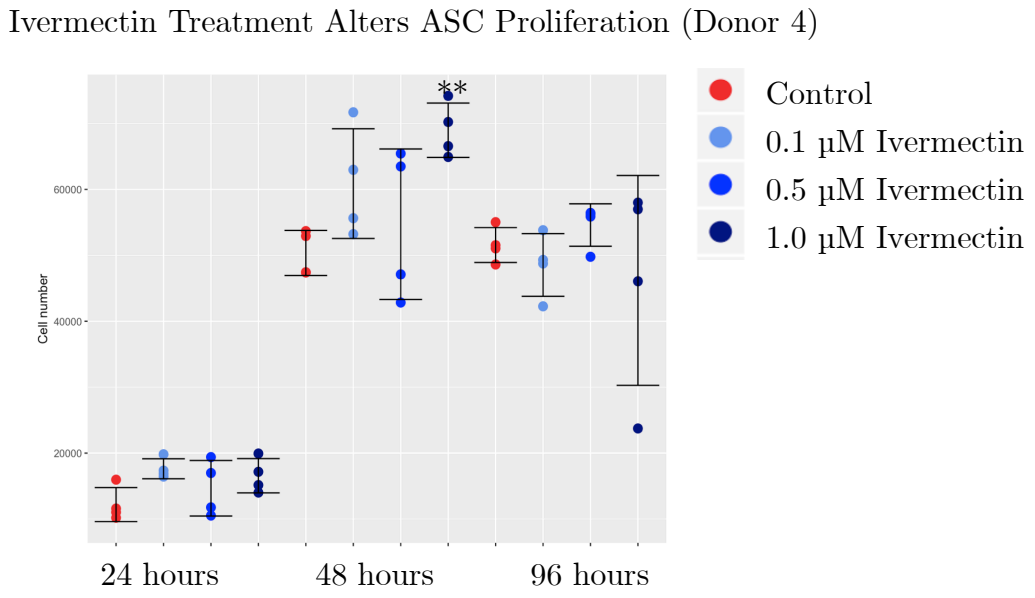

Figure 8. 2D Ivermectin Tolerance for Donor 4. A significant increase in ASC number was observed at 48 hours between the control and 1.0µM ivermectin treatment. Cell number was measured with Picogreen. Error bars represent standard deviation (ANOVA, $p < 0.01$, n=4 per treatment).

A commonly employed technique for assessing cell migration and proliferation in 2D is the scratch assay. In this technique, cells are grown to confluence in 2D before a P200 pipette tip is used to scratch a straight line down the center of each well, removing the cells from this area. The resulting scratch is then imaged over time to assess cell movement into the gap over time. A single experiment showed a decrease in scratch closure time for 0.1µM ivermectin-treated cells compared to the control with an n of 2 for the control and an n of 4 for ivermectin treatment (Figure 9). An additional experiment with n of 10 and 12 showed no significant differences in scratch closure time between the control and ivermectin treatment. However, the standard deviation of the data was very high, which may obscure underlying trends (Figure 10).

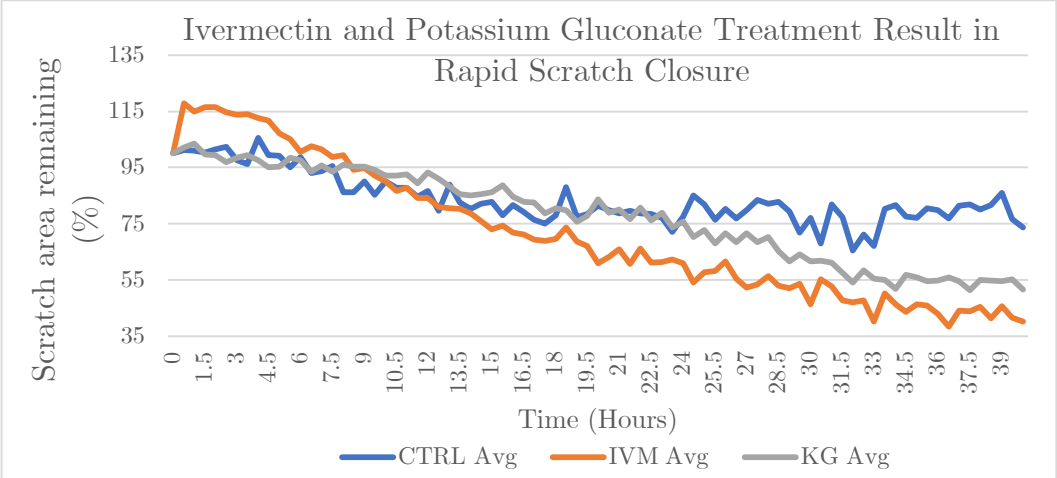

Figure 9. Ivermectin and potassium gluconate decreased scratch closure time compared to the control in a 40 hour scratch assay. Cells were seeded 24 hours before scratch was initiated. Time lapse imaging was performed on a Keyence microscope. n= 2 for control, n= 4 for 0.1µM ivermectin and 60mM potassium gluconate.

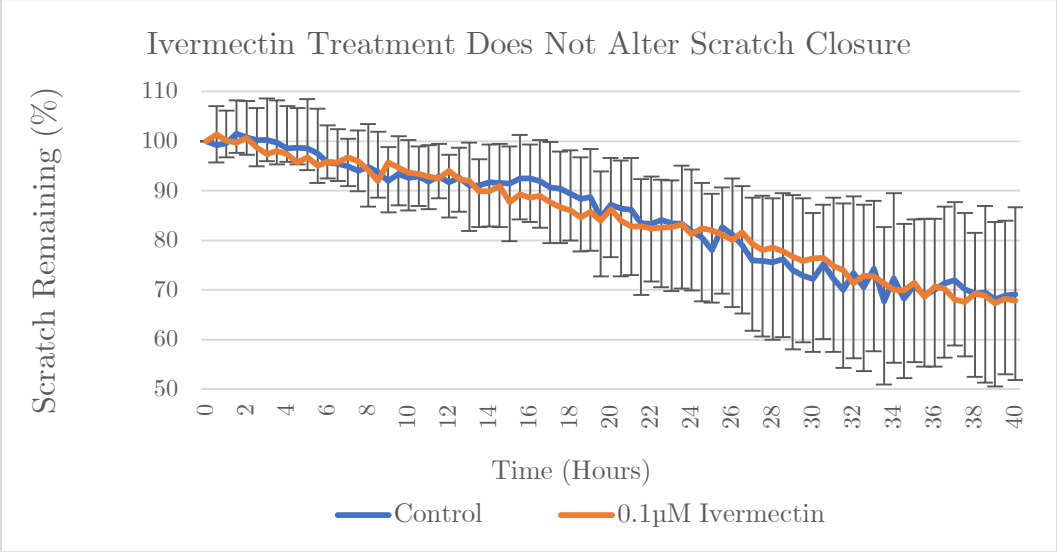

Figure 10. Ivermectin and control showed no significant differences in scratch closure time in a repeat of a scratch assay. Cells were seeded 24 hours before scratch was initiated. Time lapse imaging was performed over 40 hours on a Keyence microscope. n= 10 for control and n= 12 for 0.1µM ivermectin. Error bars represent standard deviation.

As cells grow in a 3D microenvironment in vivo and do not necessarily behave the same way as in 2D culture, it is essential to examine cell behavior in 3D. To evaluate the impact of ivermectin treatment in 3D culture, a model was developed to examine cell migration and proliferation. In this model, cells were densely seeded on two silk fibroin scaffolds before a third empty scaffold was

abutted between the two seeded scaffolds (Figure 11). Cell number was later measured in the inner and outer scaffolds as a metric of cell migration into the center scaffold and overall cell proliferation (Figure 12). This migration and proliferation assay showed a significant increase in cell number in silk scaffolds treated with 0.1µM ivermectin after 48 hours (Figure 13). However, a repeat of the experiment showed no significant difference between ivermectin treatment and the control (Figure 14). A longer term experiment showed no significant difference in cell migration or proliferation following 0.1µM ivermectin treatment 10 days (Figure 15).

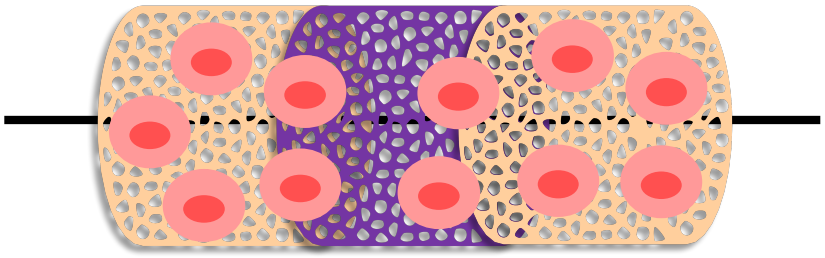

Figure 11. A schematic of the model for 3D migration and proliferation. In this model, cells are seeded on the outer (tan) scaffold and migrate into the empty (purple) scaffold. Pink circles represent ASCs.

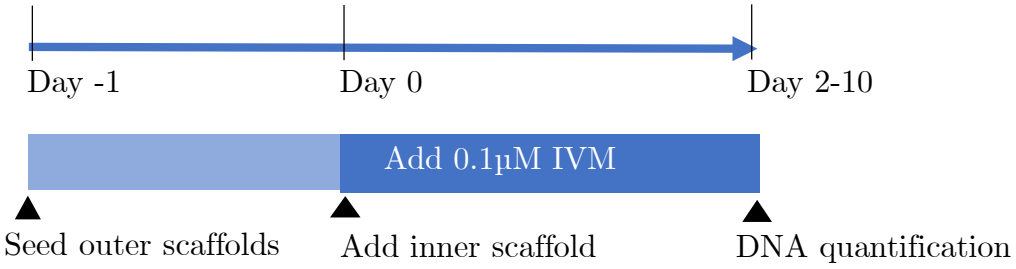

Figure 12. A timeline for the 3D migration and proliferation and proliferation assay. Cells are first seeded on silk fibroin sponges and grown for one day before a third empty scaffold was abutted between the two seeded scaffolds. Cells were allowed to migrate for 2-10 days before DNA quantification.

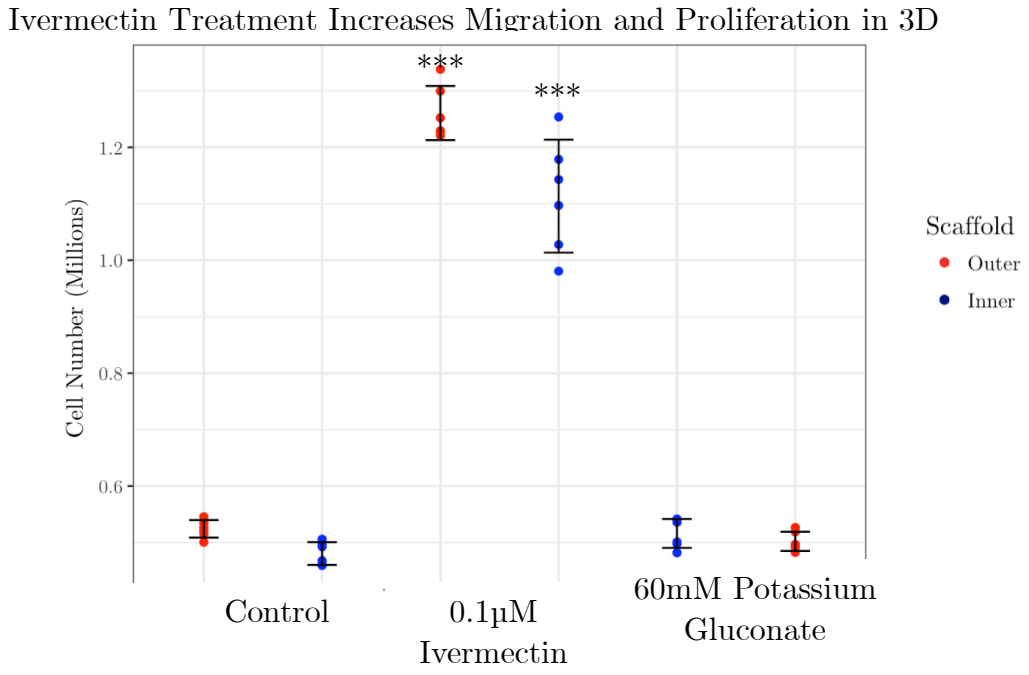

Figure 14. In a 48 hour migration and proliferation assay cell number was significantly greater in ivermectin-treated inner and outer scaffolds ASCs were seeded on a silk fibroin sponge and grown for one day prior to abutment. Cell number was measured with Picogreen after 48 hours of abutment (ANOVA, Bonferroni correction, n= 6 per group, *** p= 0.0013).

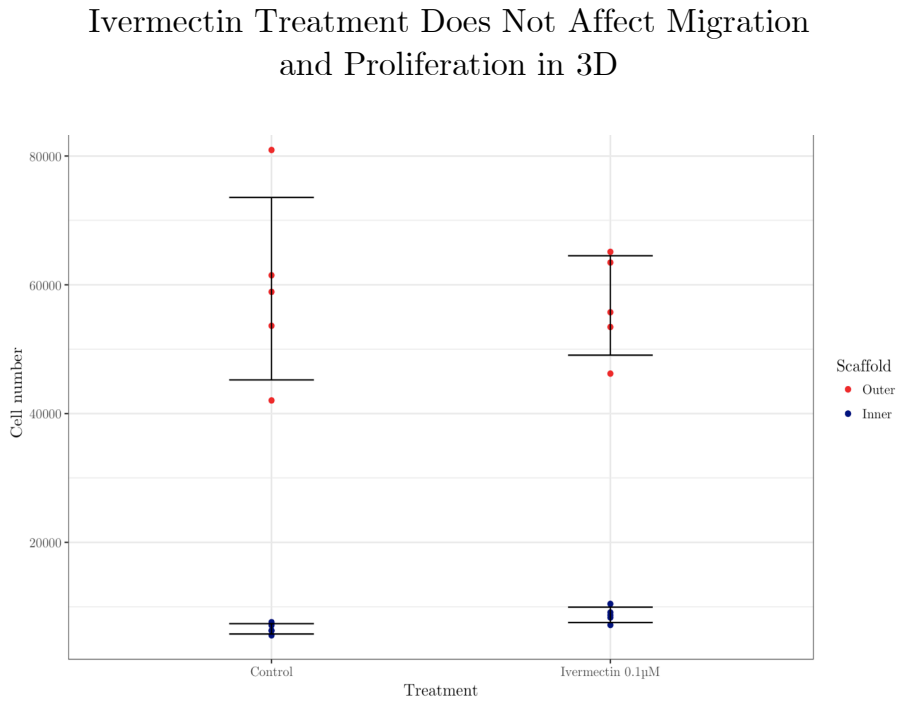

Figure 13. In a repeat of the 48 hour migration and proliferation assay, cell number in ivermectin-treated scaffolds was not significantly different than the control. Cell number was measured with Picogreen after 48 hours of abutment (ANOVA, Bonferroni correction, n= 5 per group, p > 0.05, NSD between groups).

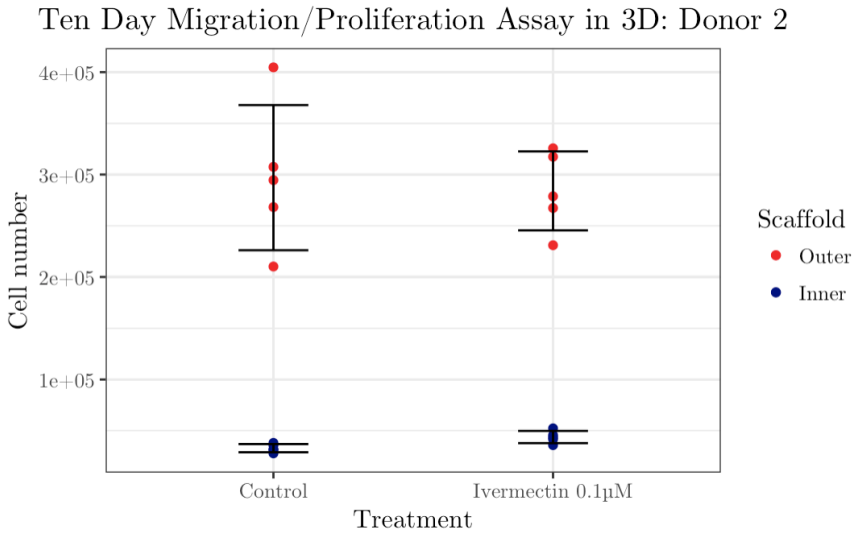

Figure 15. In a long term migration and proliferation assay, cell number in ivermectin-treated scaffolds was not significantly different than the control. Cell number was measured with Picogreen after 10 days of abutment (ANOVA, Bonferroni correction, n= 5 per group, p > 0.05, NSD between groups).

Many growth and proliferation markers are cytokines which play a role in cell migration and patterning. Therefore, to evaluate the effects of ivermectin treatment on growth and proliferation cytokine production, a RayBio C-Series Human Cytokine Antibody Array C5 was utilized to determine relative levels of secreted cytokine levels (Figure 16). Results were normalized to cell number determined by Picogreen (Figure 16). The expression of VEGF-A, IL-8, GRO a/b/g, and GRO alpha were greater in 3D than in 2D (Figure 17). However, cytokine expression did not appear to differ between drug treated samples and the controls. Many of the most highly expressed cytokines in ASCs were growth

related (Table 2). Statistical analysis was not performed as n=1 for each cytokine per treatment.

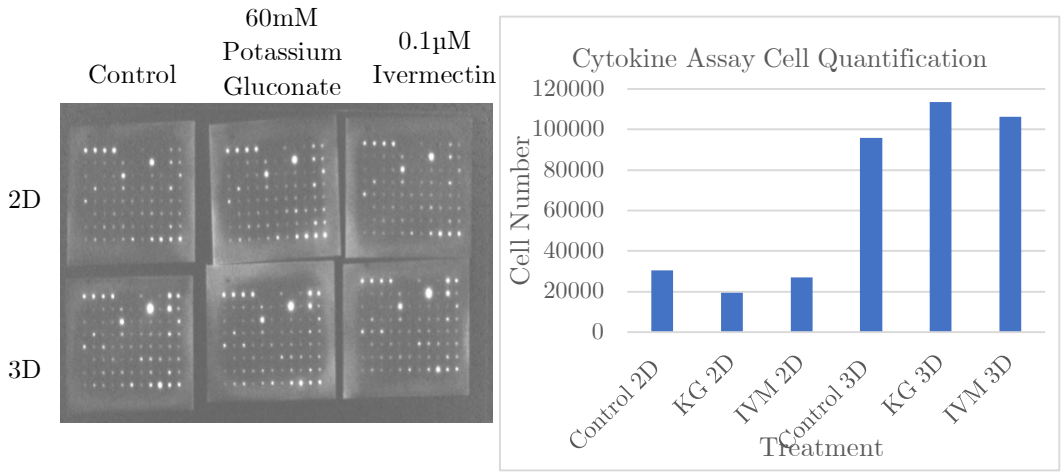

Figure 17. Media from six pooled samples each was applied to RayBio C-Series Human Cytokine Antibody Array C5 membranes as per manufacturer protocol following cell treatment with 60mM potassium gluconate or 0.1µM ivermectin. Picogreen was used to quantify cell number for normalization of cytokine data.

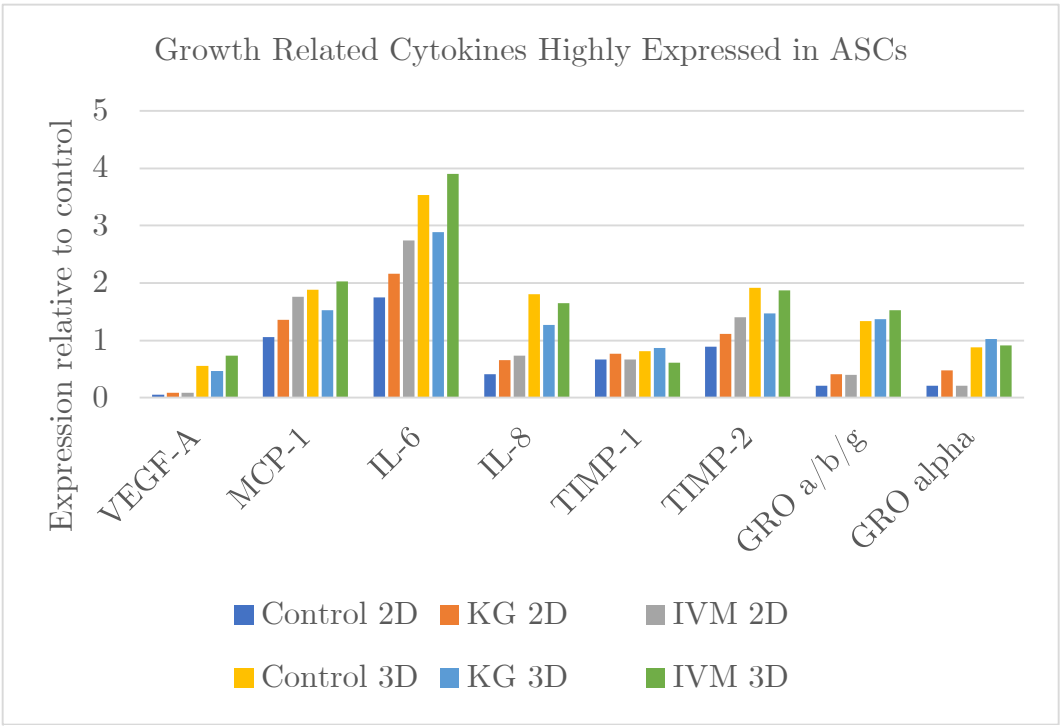

Figure 16. Many of the most highly expressed cytokines in ASCs are related to growth and proliferation. Additionally, expression levels differed between 2D and 3D samples. Most cytokines were more highly expressed in 3D, while TIMP-1 and TIMP-2 were expressed similarly in 2D and 3D.

Table 2. Functions of Most Highly Expressed Cytokines in ASCs

Cytokine	**Function**
VEGF-A	Vascular endothelial growth factor
MCP-1	Monocyte chemoattractant, produced in bone, neurons
IL-6	Can be both pro and anti-inflammatory, produced by adipocytes
IL-8	Potent promoter of angiogenesis
TIMP-1 and TIMP-2	Metastasis suppressor, inhibits ECM degradation, suppresses endothelial proliferation
GRO a/b/g	Neutrophil stimulation
GRO alpha	Mitogenic, angiogenic, wound healing, neuroprotective

Voltage Dye Analysis of ASCs Shows No Significant Change in Membrane Potential Upon Ivermectin Treatment

Ivermectin is known to open chloride channels such as GlyR, which results in an inward Cl^- current and cell hyperpolarization (Chen and Kubo, 2017). However, ASCs are not known to express GlyR; therefore, ivermectin's target in ASCs is unknown. To determine whether ivermectin's target in ASCs alters membrane potential, voltage reporter dyes were used to measure relative membrane potential. To determine the optimal voltage reporter dye for use in ASCs, four voltage reporter dyes were tested for their suitability. Each dye was used to stain ASCs per manufacturer guidelines for use in mammalian cell culture. Cells were imaged after incubation to determine which dye provided the best signal with the least background. $DiBAC_4(3)$ exhibited the greatest

background and least specificity. Di-8-ANEPPS exhibited punctate staining, indicating potential vesicular uptake. $DiSBAC_2(3)$ and SS44 (di-anionic) exhibited clear staining, with $DiSBAC_2(3)$ showing greater signal intensity around the cell body than SS44 di-anionic (Figure 18). However, $DiSBAC_2(3)$ photobleached quickly upon imaging and was not used for subsequent experiments (Data not shown).

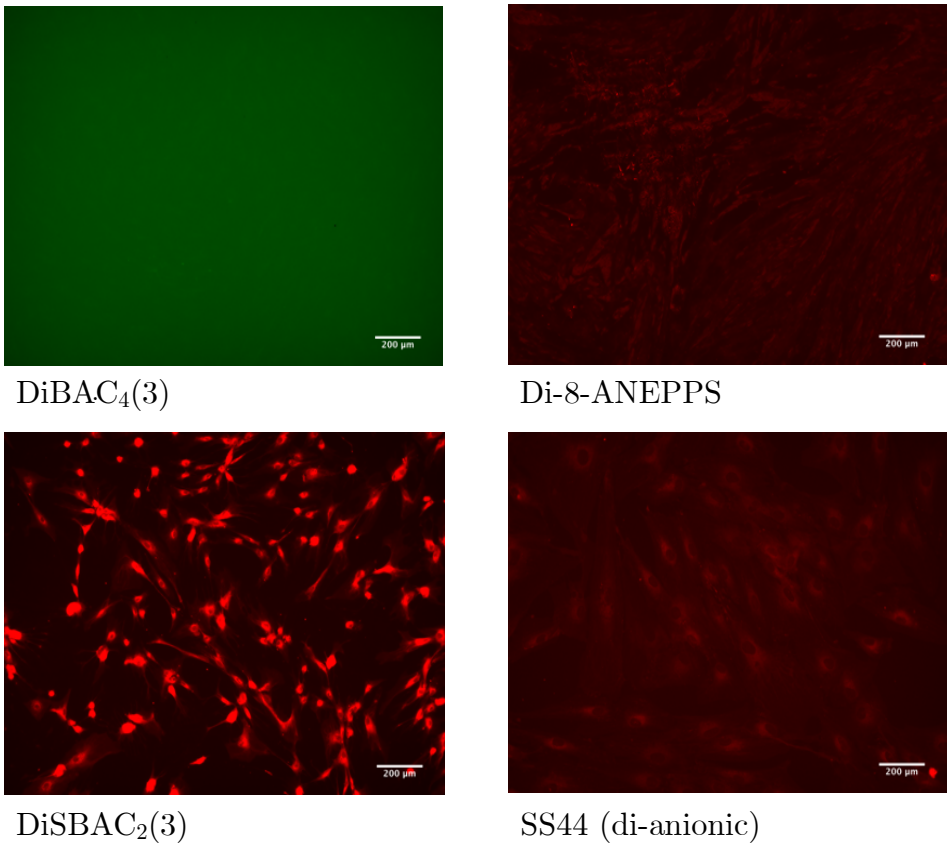

Figure 18. Comparison of four voltage reporter dyes showed that $DiSBAC_2(3)$ and SS44 (di-anionic) exhibited clearest staining, while $DiBAC_4(3)$ exhibited poor specificity and Di-8-ANEPPS exhibited punctate staining.

To evaluate the effect of ivermectin treatment on membrane potential in ASCs, cells were incubated with the voltage reporter dye SS44 (di-anionic) and resulting fluorescence was measured with a plate reader. Adipose-derived stem cells treated with ivermectin for one hour were not found to have significantly different membrane potentials in a plate reader assay with SS44 (di-anionic). The spread of the data was large for both groups. The control data was not skewed while the ivermectin-treated group showed right skewness (Figure 19).

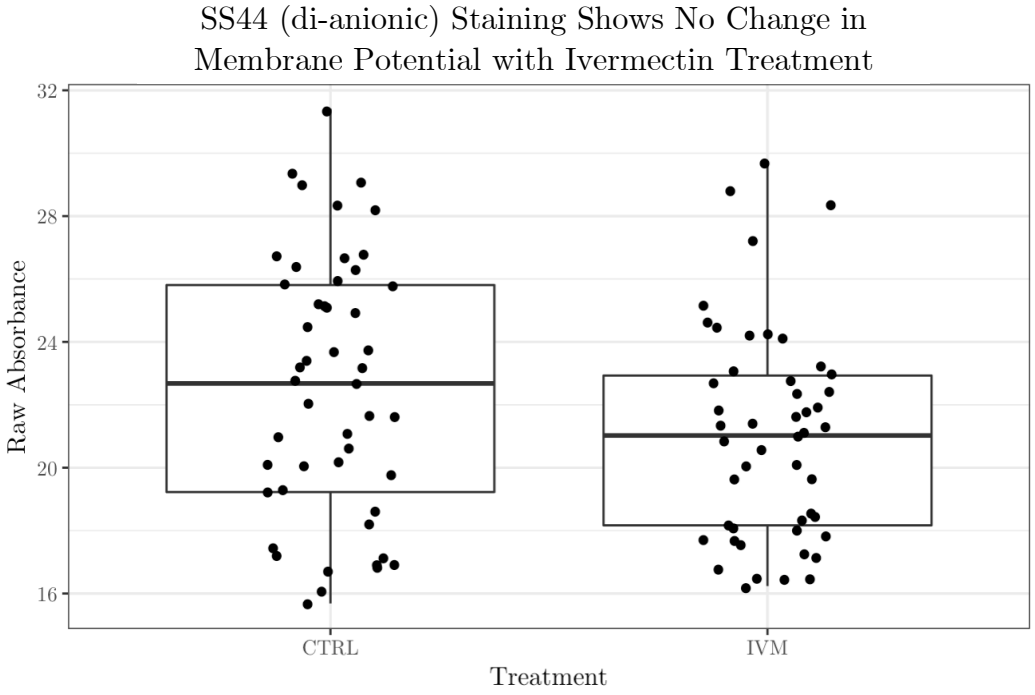

Figure 19. No significant difference was observed between mean fluorescence in ASCs treated with 0.1µM ivermectin for one hour, indicating no significant difference in membrane potential. Samples were stained with SS44 (di-anionic) for one hour. Samples were excited at 628 nm and emission was measured at 712 nm (Welch's T-test, n=36 per group, p> 0.05).

Patch clamp measurement of ASCs treated with ivermectin shows no difference in membrane potential

To quantitatively measure membrane potential following ivermectin treatment, patch clamp was utilized. Cells were seeded 48 hours in advance of patch clamping and were treated with 0.1µM ivermectin. Cells were briefly trypsinized then allowed to recover for five minutes at 37°C before patch clamping (Figure 20). Membrane potential was found to be depolarized in several cells treated with ivermectin for both three hours and five days in a set of experiments that were not day matched (Figure 21a). However, a day-matched experiment with a greater number of cells showed no significant differences between ASCs treated with 0.1µM ivermectin and the control (Figure 21b and c). The normalized distributions of both control and treated membrane potentials were also similar (Figure 21d and e).

Figure 20. A timeline for patch clamp experiments. ASCs were seeded 48 hours before experimentation and treated with 0.1µM ivermectin. Cells were briefly trypsinized before experimentation to minimize cell flatness.

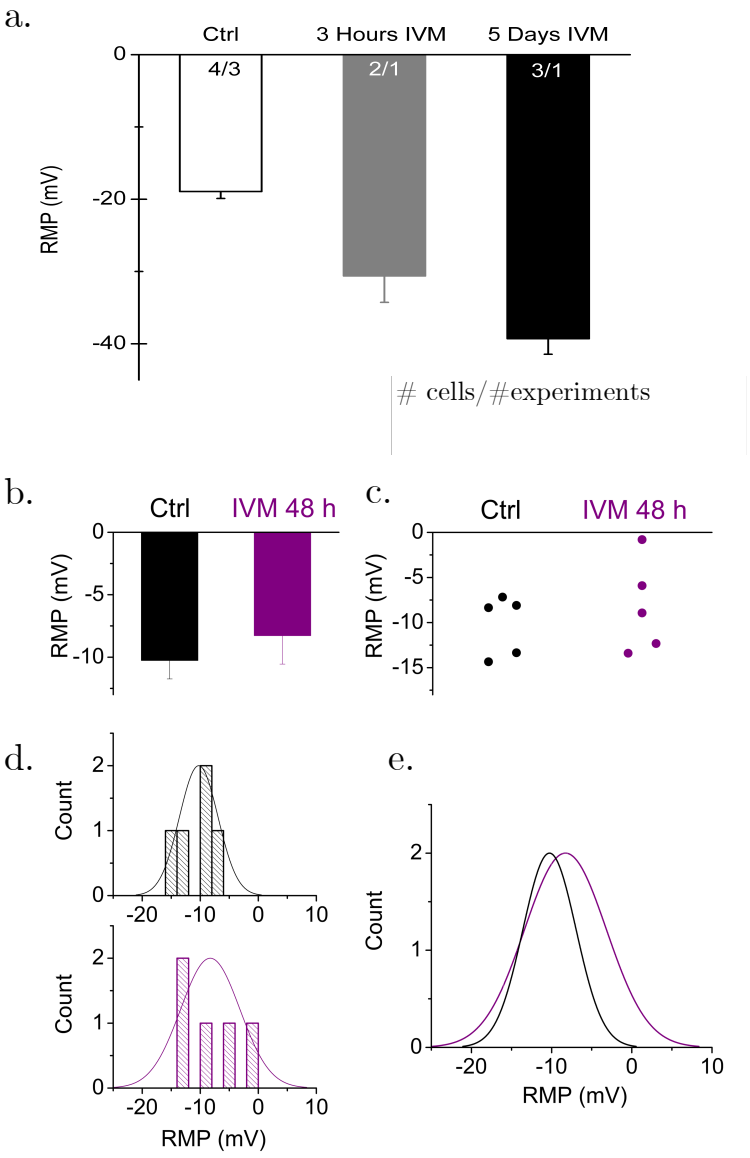

Figure 21. Resting membrane potential is unaltered by treatment with 0.1µM ivermectin. a) In a set of experiments that was not day-matched, cells treated with 0.1µM ivermectin for three hours or five days showed hyperpolarized resting membrane potential. b) The average resting membrane potential for cells treated with 0.1µM ivermectin for 48 hours was not shown to significantly differ. Error bars represent the mean +/- SEM c) The spread of control and ivermectin-treated membrane potentials was similar. d and e) When a normal distribution is approximated over the membrane potentials measured, the distributions are very similar between ivermectin treatment and the control.

Discussion

Adipose-derived stem cells have significant potential for use in clinical therapies due to their potential for autogenic transplantation. Therefore, it is imperative to determine mechanisms by which ASCs pattern and migrate such that these behaviors can be exploited for therapeutic purposes. This project aimed to examine whether ivermectin can be utilized as an electroceutical drug to alter ASC behavior.

Four different drugs were assessed for their effects on metabolic activity with WST-1, an assay that measures mitochondrial function. Because pinacidil and glibenclamide were found to significantly decrease metabolic activity, which is indicative of toxicity (Figure 4). Therefore, future experiments excluded these drugs. Ivermectin was not found affect to metabolic activity (Figure 5). Picogreen was also used to measure cell number via DNA quantification. While Picogreen does not provide metabolic data, it is indicative of proliferation because the DNA content in each cell is the same. As it is possible that ivermectin affects proliferation but not mitochondrial metabolism, both assays were used in conjunction.

The effects of ivermectin treatment in 2D for three different donors was assessed and donor to donor variability was observed in responses to ivermectin (Figures 6, 7, 8). Donor to donor variability in ASCs is well known to occur and many factors can impact ASC behavior, including genetic variation, patient metabolic state, and epigenetic variation (Sundelacruz et al., 2015).

Ivermectin's effects on cell migration were also assessed through 2D scratch assay and time lapse imaging. While an early experiment showed that ivermectin-treated cells closed the scratch faster than control, the number of experimental replicates in this study was too low to verify significance (Figure 9). This result was not reproducible in a later experiment with a larger n. The variability between replicates was also very high, which could obscure any underlying trends (Figure 10).

Ivermectin treatment was shown to significantly increase cell migration and proliferation in 3D after 48 hours in a single experiment (Figure 13), but this result was not reproducible (Figure 14). It is possible that the variability in 2D and 3D proliferation data is due to the presence of growth factors in the expansion media. Growth factors were withdrawn upon experimentation. However, it is possible that the effects of the growth factors persist for several days following exposure. Because ASCs are primary cell lines and they are known to lose stem cell character with passaging it is possible that passage number affected results (Choi et al., 2010). However, care was taken to not use cells P6, which is within the number of passages that ASCs should retain their stem cell character.

Early voltage reporter experiments with the dye SS44 (di-anionic) showed that the mean membrane potential was not significantly altered in hASCs treated with 0.1μM ivermectin for one hour (Figure 19). However, it is possible that the voltage dye protocol utilized was not optimized enough to show significant differences. Therefore, patch clamp was utilized to quantitatively measure resting membrane potential. In an early experiment with a few cells, ivermectin treatment

appeared to induce depolarization in a time dependent manner (Figure 21a). However, this data was not time matched as the ivermectin-treated and control cells were measured on separate days. A later, time-matched experiment showed that the resting potentials of cells treated with 0.1μM ivermectin were very similar (Figure 21b). Given the patch clamp results, it appears that the membrane potential of hASCs treated with ivermectin may not be altered. To verify this finding, additional patch clamp experiments could be performed in chloride-free media. The media used in these experiments contained FBS, which is an undefined supplement. Lot to lot variation in chloride concentration can occur, which may introduce variability into membrane potential.

If membrane potential is not altered by ivermectin in ASCs, it does not mean that ivermectin does not have a physiological effect on adipose-derived stem cells. Ivermectin is known to have multiple mammalian targets, including the channels GlyR, P2X4, and GIRK and the transcriptional regulator FXR (Table 1). Therefore, it is possible that ivermectin treatment does not alter membrane potential in hASCs if the target is not an ion channel. Ion channel expression in hASCs is poorly characterized. However, there is evidence that hASCs express Kv1.1, Kv2.1, Kv1.5, Kv7.3, Kv11.1, hEAG1, MaxiK, KCNN3, KCNN4 Kv1.4, Kv4.1, Kv4.2, Kv4.3, and hNE-N (Bai et al., 2007; Forostyak et al., 2016), and importantly P2X (Forostyak et al., 2016). Therefore, it is possible that ivermectin's target in ASCs is P2X4.

Because ivermectin treatment was shown to alter growth-related cytokine production in hASCs, it is possible that ivermectin plays a role in altering hASC

growth physiology. Additionally, cytokine production was found to differ in 2D vs 3D (Figure 17). Future studies can be undertaken to further investigate the role of membrane potential modulation on cell response in 3D. Additionally, it is important to investigate tissue response rather than single cell type response. While ASCs alone were used for these experiments, co-cultures or even cells derived from whole tissue could be grown in 3D to evaluate the effects on multiple cell types. ASCs are known to play a prominent role in paracrine signaling in the vascular niche of adipose tissue (Domenis et al., 2017), and it is conceivable that membrane potential modulation could affect this signaling.

ASCs hold the potential for numerous clinical applications, as is evidenced by the many clinical trials currently involving ASCs (Zuk, 2013). Therefore, the study of cell patterning in ASCs is a field of study that holds much relevance for future cell-based and tissue-engineered therapeutics.

Future Directions

The promising role of bioelectricity in ASC patterning is still largely unexplored. Therefore, several future experiments can be undertaken to address the impacts of bioelectric signaling on ASC biology. Specifically, the mechanisms by which ASC behavior is altered upon membrane potential alteration are currently unstudied.

While ivermectin was primarily used in this study, there are many other ways to modulate membrane potential that could be explored in the future. Optogenetic techniques are rising in popularity for the modulation of membrane potential, as they are highly versatile and can be quickly adapted for specific applications (Ferenczi et al., 2016). Optogenetic techniques employ the use of light-sensitive ion channels derived from bacteria which can be controlled with specific wavelengths of light, leading to a change in membrane potential due to changes in ion conductance (Boyden et al., 2005; Nagel et al., 2003; Zhang et al., 2007). These techniques can be used to specifically and temporally control membrane potential in ASCs, making it a powerful method for future studyies. Alternatively, upon identification of a channel target, specific channel knockdowns could be performed with shRNAs to assess the effects of specific channel expression on membrane potential and cell behavior.

To assess the impact of specific membrane potential altering drugs on 2D cell migration and proliferation, cell cycle synchronization could be used before a scratch assay to observe cell response without variability due to differences in cell cycle stage.

Additionally, future experiments could be performed to assess the effects of ASC expansion with growth factors on response to membrane potential-altering drugs. Because ASCs can only be passaged a limited number of times before losing key ASC markers, it is important to determine whether drug exposure varies the number of passages that the cells their stem cell markers.

Future experiments with chloride free media could be performed to assess effects of ivermectin treatment on ASC membrane potential. This would allow for the addition of known amounts of chloride with and without ivermectin treatment to determine if membrane potential and cell behavior is altered in a chloride-dependent manner. Additionally, patch clamping with a perfusion system and temperature control would provide a more stable and customizable setup for experimentation. This would allow for the measurement of a single cell's membrane potential during acute treatment with ivermectin and allow for the assessment of acute membrane potential response. Additionally, a perfusion system would allow for temperature control, which would make data more consistent due to lack of changing temperature effects. Another future direction would be to correlate voltage reporter dyes with patch clamp data to generate a way to quantify voltage dye readings in ASCs. This would increase the throughput of membrane potential readings and allow for rapid screening of drugs for their effects on membrane potential.

The impact of bioelectric signaling on the ASC transcriptome and proteome has never been studied. However, the transcriptome and proteome could shed light on the transduction mechanisms that are impacted by bioelectric

signaling in ASCs. To assess the effects of membrane potential alteration on the transcriptome and proteome, RNA-seq and mass spectrometry could be performed after membrane potential alteration using either drugs or optogenetic methods. Understanding the transduction mechanisms for bioelectric signals will allow for more precise manipulation of ASC patterning for future tissue engineering and regenerative applications.

Bibliography

Abbott, R.D., Kimmerling, E.P., Cairns, D.M., and Kaplan, D.L. (2016). Silk as a Biomaterial to Support Long-Term Three-Dimensional Tissue Cultures. ACS Appl. Mater. Interfaces *8*, 21861–21868.

Alberts, B., Johnson, A., Lewis, J., Raff, M., Roberts, K., and Walter, P. (2002). Ion Channels and the Electrical Properties of Membranes.

Ashraf, S., and Prichard, R. (2016). Ivermectin exhibits potent anti-mitotic activity. Vet. Parasitol. *226*, 1–4.

Bai, X., Ma, J., Pan, Z., Song, Y.-H., Freyberg, S., Yan, Y., Vykoukal, D., and Alt, E. (2007). Electrophysiological properties of human adipose tissue-derived stem cells. Am. J. Physiol. Cell Physiol. *293*, C1539-50.

Blackiston, D.J., McLaughlin, K.A., and Levin, M. (2009). Bioelectric controls of cell proliferation. Cell Cycle Georget. Tex *8*, 3519–3528.

Boyden, E.S., Zhang, F., Bamberg, E., Nagel, G., and Deisseroth, K. (2005). Millisecond-timescale, genetically targeted optical control of neural activity. Nat. Neurosci. *8*, 1263–1268.

Bunnell, B.A., Flaat, M., Gagliardi, C., Patel, B., and Ripoll, C. (2008). Adipose-derived stem cells: isolation, expansion and differentiation. Methods San Diego Calif *45*, 115–120.

Carpenter, A.E., Jones, T.R., Lamprecht, M.R., Clarke, C., Kang, I.H., Friman, O., Guertin, D.A., Chang, J.H., Lindquist, R.A., Moffat, J., et al. (2006). CellProfiler: image analysis software for identifying and quantifying cell phenotypes. Genome Biol. *7*, R100.

Chen, I.-S., and Kubo, Y. (2017). Ivermectin and its target molecules: shared and unique modulation mechanisms of ion channels and receptors by ivermectin. J. Physiol. n/a-n/a.

Choi, J.H., Gimble, J.M., Lee, K., Marra, K.G., Rubin, J.P., Yoo, J.J., Vunjak-Novakovic, G., and Kaplan, D.L. (2010). Adipose tissue engineering for soft tissue regeneration. Tissue Eng. Part B Rev. *16*, 413–426.

Choi, J.H., Bellas, E., Vunjak-Novakovic, G., and Kaplan, D.L. (2011). Adipogenic Differentiation of Human Adipose-Derived Stem Cells on 3D Silk Scaffolds. In Adipose-Derived Stem Cells, (Humana Press, Totowa, NJ), pp. 319–330.

Collins, M.N., and Birkinshaw, C. (2013). Hyaluronic acid based scaffolds for tissue engineering—A review. Carbohydr. Polym. *92*, 1262–1279.

Crump, A., and Omura, S. (2011). Ivermectin, 'Wonder drug' from Japan: the human use perspective. Proc. Jpn. Acad. Ser. B Phys. Biol. Sci. *87*, 13–28.

Dhaliwal, A. (2018). 3D Cell Culture: A Review. Mater. Methods.

Domenis, R., Quaglia, S., Cifù, A., Pistis, C., Fabris, M., Moretti, M., Vicario, A., Niazi, K.R., and Curcio, F. (2017). The immunomodulatory properties of adipose mesenchymal stem cell-derived exosomes are induced by inflammatory cytokines. FASEB J. *31*, 981.5-981.5.

Escobar, C.H., and Chaparro, O. (2016). Xeno-Free Extraction, Culture, and Cryopreservation of Human Adipose-Derived Mesenchymal Stem Cells. Stem Cells Transl. Med. *5*, 358–365.

Ferenczi, E.A., Vierock, J., Atsuta-Tsunoda, K., Tsunoda, S.P., Ramakrishnan, C., Gorini, C., Thompson, K., Lee, S.Y., Berndt, A., Perry, C., et al. (2016). Optogenetic approaches addressing extracellular modulation of neural excitability. Sci. Rep. *6*, 23947.

Forostyak, O., Butenko, O., Anderova, M., Forostyak, S., Sykova, E., Verkhratsky, A., and Dayanithi, G. (2016). Specific profiles of ion channels and ionotropic receptors define adipose- and bone marrow derived stromal cells. Stem Cell Res. *16*, 622–634.

Frese, L., Dijkman, P.E., and Hoerstrup, S.P. (2016). Adipose Tissue-Derived Stem Cells in Regenerative Medicine. Transfus. Med. Hemotherapy *43*, 268–274.

Gir, P., Oni, G., Brown, S.A., Mojallal, A., and Rohrich, R.J. (2012). Human adipose stem cells: current clinical applications. Plast. Reconstr. Surg. *129*, 1277–1290.

Glowacki, J., and Mizuno, S. (2008). Collagen scaffolds for tissue engineering. Biopolymers *89*, 338–344.

González, M.A., Gonzalez-Rey, E., Rico, L., Büscher, D., and Delgado, M. (2009). Adipose-derived mesenchymal stem cells alleviate experimental colitis by inhibiting inflammatory and autoimmune responses. Gastroenterology *136*, 978–989.

Gonzalez-Rey, E., Gonzalez, M.A., Varela, N., O'Valle, F., Hernandez-Cortes, P., Rico, L., Büscher, D., and Delgado, M. (2010). Human adipose-derived mesenchymal stem cells reduce inflammatory and T cell responses and induce regulatory T cells in vitro in rheumatoid arthritis. Ann. Rheum. Dis. *69*, 241–248.

Hadden, W.J., Young, J.L., Holle, A.W., McFetridge, M.L., Kim, D.Y., Wijesinghe, P., Taylor-Weiner, H., Wen, J.H., Lee, A.R., Bieback, K., et al. (2017). Stem cell migration and mechanotransduction on linear stiffness gradient hydrogels. Proc. Natl. Acad. Sci. U. S. A. *114*, 5647–5652.

Hassan, W.U., Greiser, U., and Wenxin Wang (2014). Role of adipose-derived stem cells in wound healing. Wound Repair Regen. Off. Publ. Wound Heal. Soc. Eur. Tissue Repair Soc. *22*, 313–325.

Iyyanki, T., Hubenak, J., Liu, J., Chang, E.I., Beahm, E.K., and Zhang, Q. (2015). Harvesting Technique Affects Adipose-Derived Stem Cell Yield. Aesthet. Surg. J. *35*, 467–476.

Johal, K.S., Lees, V.C., and Reid, A.J. (2015). Adipose-derived stem cells: selecting for translational success. Regen. Med. *10*, 79–96.

Kim, W.-S., Park, B.-S., Sung, J.-H., Yang, J.-M., Park, S.-B., Kwak, S.-J., and Park, J.-S. (2007). Wound healing effect of adipose-derived stem cells: A critical role of secretory factors on human dermal fibroblasts. J. Dermatol. Sci. *48*, 15–24.

Lan, J.-Y., Williams, C., Levin, M., and Black, L.D. (2014). Depolarization of Cellular Resting Membrane Potential Promotes Neonatal Cardiomyocyte Proliferation In Vitro. Cell. Mol. Bioeng. *7*, 432–445.

Lee, K.Y., and Mooney, D.J. (2012). Alginate: properties and biomedical applications. Prog. Polym. Sci. *37*, 106–126.

Levin, M. (2014). Molecular bioelectricity: how endogenous voltage potentials control cell behavior and instruct pattern regulation in vivo. Mol. Biol. Cell *25*, 3835–3850.

Levin, M., Pezzulo, G., and Finkelstein, J.M. (2017). Endogenous Bioelectric Signaling Networks: Exploiting Voltage Gradients for Control of Growth and Form. Annu. Rev. Biomed. Eng. *19*, 353–387.

Liang, C.-C., Park, A.Y., and Guan, J.-L. (2007). In vitro scratch assay: a convenient and inexpensive method for analysis of cell migration in vitro. Nat. Protoc. *2*, 329–333.

Lindroos, B., Suuronen, R., and Miettinen, S. (2011). The potential of adipose stem cells in regenerative medicine. Stem Cell Rev. *7*, 269–291.

Lodish, H., Berk, A., Zipursky, S.L., Matsudaira, P., Baltimore, D., and Darnell, J. (2000). Overview of Membrane Transport Proteins.

McKee, C., and Chaudhry, G.R. (2017). Advances and challenges in stem cell culture. Colloids Surf. B Biointerfaces *159*, 62–77.

Meyers, J.I., Gray, M., Kuklinski, W., Johnson, L.B., Snow, C.D., Black, W.C., Partin, K.M., and Foy, B.D. (2015). Characterization of the target of ivermectin, the glutamate-gated chloride channel, from Anopheles gambiae. J. Exp. Biol. *218*, 1478–1486.

Mildmay-White, A., and Khan, W. (2017). Cell Surface Markers on Adipose-Derived Stem Cells: A Systematic Review. Curr. Stem Cell Res. Ther. *12*, 484–492.

Miller, E.W. (2016). Small molecule fluorescent voltage indicators for studying membrane potential. Curr. Opin. Chem. Biol. *33*, 74–80.

Na, Y.K., Ban, J.-J., Lee, M., Im, W., and Kim, M. (2017). Wound healing potential of adipose tissue stem cell extract. Biochem. Biophys. Res. Commun. *485*, 30–34.

Nagel, G., Szellas, T., Huhn, W., Kateriya, S., Adeishvili, N., Berthold, P., Ollig, D., Hegemann, P., and Bamberg, E. (2003). Channelrhodopsin-2, a directly light-gated cation-selective membrane channel. Proc. Natl. Acad. Sci. U. S. A. *100*, 13940–13945.

Özkucur, N., Quinn, K.P., Pang, J.C., Du, C., Georgakoudi, I., Miller, E., Levin, M., and Kaplan, D.L. (2015). Membrane potential depolarization causes

alterations in neuron arrangement and connectivity in cocultures. Brain Behav. *5*, 24–38.

Pai, V.P., Aw, S., Shomrat, T., Lemire, J.M., and Levin, M. (2012). Transmembrane voltage potential controls embryonic eye patterning in Xenopus laevis. Development *139*, 313–323.

Sachs, H.G., Stambrook, P.J., and Ebert, J.D. (1974). Changes in membrane potential during the cell cycle. Exp. Cell Res. *83*, 362–366.

Schindelin, J., Arganda-Carreras, I., Frise, E., Kaynig, V., Longair, M., Pietzsch, T., Preibisch, S., Rueden, C., Saalfeld, S., Schmid, B., et al. (2012). Fiji: an open-source platform for biological-image analysis. Nat. Methods *9*, 676–682.

Sharmeen, S., Skrtic, M., Sukhai, M.A., Hurren, R., Gronda, M., Wang, X., Fonseca, S.B., Sun, H., Wood, T.E., Ward, R., et al. (2010). The antiparasitic agent ivermectin induces chloride-dependent membrane hyperpolarization and cell death in leukemia cells. Blood *116*, 3593–3603.

Sundelacruz, S., Levin, M., and Kaplan, D.L. (2008). Membrane Potential Controls Adipogenic and Osteogenic Differentiation of Mesenchymal Stem Cells. PLOS ONE *3*, e3737.

Sundelacruz, S., Levin, M., and Kaplan, D.L. (2015). Comparison of the depolarization response of human mesenchymal stem cells from different donors. Sci. Rep. *5*.

Thurber, A.E., Omenetto, F.G., and Kaplan, D.L. (2015). In vivo bioresponses to silk proteins. Biomaterials *71*, 145–157.

Tsuji, W., Rubin, J.P., and Marra, K.G. (2014). Adipose-derived stem cells: Implications in tissue regeneration. World J. Stem Cells *6*, 312–321.

Tyagi, S., Gupta, P., Saini, A.S., Kaushal, C., and Sharma, S. (2011). The peroxisome proliferator-activated receptor: A family of nuclear receptors role in various diseases. J. Adv. Pharm. Technol. Res. *2*, 236–240.

Vepari, C., and Kaplan, D.L. (2007). Silk as a Biomaterial. Prog. Polym. Sci. *32*, 991–1007.

Wolstenholme, A.J. (2011). Ion channels and receptor as targets for the control of parasitic nematodes. Int. J. Parasitol. Drugs Drug Resist. *1*, 2–13.

Wolstenholme, A.J. (2012). Glutamate-gated Chloride Channels. J. Biol. Chem. *287*, 40232–40238.

Wolstenholme, A.J., and Rogers, A.T. (2005). Glutamate-gated chloride channels and the mode of action of the avermectin/milbemycin anthelmintics. Parasitology *131 Suppl*, S85-95.

Wu, Y., Chen, L., Scott, P.G., and Tredget, E.E. (2007). Mesenchymal stem cells enhance wound healing through differentiation and angiogenesis. Stem Cells Dayt. Ohio *25*, 2648–2659.

Young, D.A., Choi, Y.S., Engler, A.J., and Christman, K.L. (2013). Stimulation of adipogenesis of adult adipose-derived stem cells using substrates that mimic the stiffness of adipose tissue. Biomaterials *34*, 8581–8588.

Zanzouri, M., Lauritzen, I., Duprat, F., Mazzuca, M., Lesage, F., Lazdunski, M., and Patel, A. (2006). Membrane Potential-regulated Transcription of the Resting K+ Conductance TASK-3 via the Calcineurin Pathway. J. Biol. Chem. *281*, 28910–28918.

Zhang, F., Wang, L.-P., Brauner, M., Liewald, J.F., Kay, K., Watzke, N., Wood, P.G., Bamberg, E., Nagel, G., Gottschalk, A., et al. (2007). Multimodal fast optical interrogation of neural circuitry. Nature *446*, 633–639.

Zhang, T., Lin, S., Shao, X., Shi, S., Zhang, Q., Xue, C., Lin, Y., Zhu, B., and Cai, X. (2018). Regulating osteogenesis and adipogenesis in adipose-derived stem cells by controlling underlying substrate stiffness. J. Cell. Physiol. *233*, 3418–3428.

Zhao, Y., Inayat, S., Dikin, D.A., Singer, J.H., Ruoff, R.S., and Troy, J.B. (2009). Patch clamp technique: Review of the current state of the art and potential contributions from nanoengineering: Proc. Inst. Mech. Eng. Part N J. Nanoeng. Nanosyst.

Zuk, P. (2013). Adipose-Derived Stem Cells in Tissue Regeneration: A Review.

Zuk, P.A., Zhu, M., Ashjian, P., De Ugarte, D.A., Huang, J.I., Mizuno, H., Alfonso, Z.C., Fraser, J.K., Benhaim, P., and Hedrick, M.H. (2002). Human Adipose Tissue Is a Source of Multipotent Stem Cells. Mol. Biol. Cell *13*, 4279–4295.

Acknowledgements

Many thanks to my thesis committee: Dr. David Kaplan, Dr. Michael Levin, and Dr. Yu-Ting Dingle for guiding my research. I also wish to thank my Kaplan Lab mentors: Dr. Shreyas Jadhav, Dr. Rosalyn Abbott, and Dr. Yu-Ting Dingle for teaching me so many fundamental skills that went into the making of this thesis. I wish to specially acknowledge Dr. Yu-Ting Dingle for excellent mentorship throughout the last year. I would like to thank Dr. Mattia Bonzanni for generously performing all electrophysiological experiments reported in this thesis. Dr. Dany Adams provided the SS44 (di-anionic) dye used in membrane potential measurements. Marcello DeLuca and Martha Rimniceanu also helped significantly with feedback and revisions on drafts. This work was generously funded by the Paul G. Allen Foundation.

Appendix: Detailed Materials and Methods

Adipose-Derived Stem Cell Media Preparation

Materials for Adipose-Derived Stem Cell Media Preparation		
Product	**Vendor**	**Catalog Number**
DMEM/F-12 with GlutaMAX™ supplement (10x500mL)	ThermoFisher	10565042
Antibiotic-Antimycotic, 100X	ThermoFisher	15240062
FBS 500mL	ThermoFisher	10437-028
100 µg EGF Recombinant Human Protein	ThermoFisher	PHG0311
Recombinant Human FGF basic (R&D)	Fisher	233FB025
Recombinant Human TGF-beta 1 Protein 2µg	R&D Systems	240-B-002

1. EGF, FGF, and TGF-B1 were reconstituted according to manufacturer instructions. EGF was reconstituted to 0.1mg/mL concentration in PBS. FGF was reconstituted to 100µg/mL in 1mM acetic acid with 0.1mg/mL BSA. TGF-B1 was reconstituted to 20µg/mL in sterile 4mM HCl with 1mg/mL BSA. All growth factors were aliquoted into 20µL aliquots in small Eppendorf tubes and stored at -20°C.
2. 50mL FBS was aliquoted into 50mL conical tubes and stored at -20°C.
3. 5mL anti-anti was aliquoted into 15mL conical tubes and stored at -20°C.
4. To prepare media, 50mL was removed from a new bottle of DMEM/F12 GlutaMAX.
5. 450mL DMEM/F12, 50mL FBS, and 5mL anti-anti were mixed in the top of a 500mL 0.2µm vacuum filter bottle.
6. Media was filtered and stored at 4°C.
7. EGF at 5ng/mL, bFGF at 1ng/mL, and TGF-B at 0.25ng/mL were added directly to media before use in culture.

Adipose-Derived Stem Cell Culture (Adapted from Lonza Poietics™ human adipose derived stem cells (ADSC) Instructions for use)

Materials		
Product	**Vendor**	**Catalog Number**
Adipose-Derived Stem Cells	Lonza	PT-5006
Adipose-Derived Stem Cell Media	See Adipose-Derived Stem Cell Media Preparation	N/A

1. Adipose-derived stem cells purchased from Lonza were removed from liquid nitrogen storage thawed for less than one minute in a 37°C water bath.
2. Cells were gently suspended in 10mL pre-warmed ASC media and spun down at 150g for 5 minutes.
3. The supernatant was gently aspirated and cells were gently resuspended in an additional 10mL pre-warmed media.
4. Cells were counted and assessed for viability with Trypan Blue, then seeded at 5000 cells/cm^2 density in flasks.
5. Cells were grown and expanded in DMEM/F12 containing 10% fetal bovine serum, 1% antibiotic-antimycotic (Gibco), 5ng/mL EGF, 1ng/mL bFGF and 0.25ng/mL TGF-B (R&D Systems). EGF, bFGF and TGF-B were used for cell expansion only and withdrawn upon experimentation. Media was changed every 72 hours.
6. Cells were cultured in a humidified cell culture incubator at 37°C with 5% CO^2 and passaged at 90% confluence. Cells were used for experimentation were between P2-P6.

Preparation of Ivermectin and Potassium Gluconate

Materials		
Product	**Vendor**	**Catalog Number**
Ivermectin	Sigma	18898-250MG
Potassium Gluconate	Sigma	P1847-100G

Ivermectin

1. To prepare ivermectin stock, ivermectin powder was dissolved in DMSO for a stock concentration of 5mM and stored at 4°C.
2. To prepare ivermectin for cell culture use, the 5mM stock was first diluted 1:100 in cell culture media for a concentration of 50μM to avoid pipetting small volumes before further dilution in cell culture media to 0.1-1.0μM working concentration.

Potassium Gluconate

1. To prepare potassium gluconate stock, potassium gluconate powder was dissolved in deionized water and 0.2μM filter sterilized for a stock concentration of 1M and stored at 4°C.
2. To prepare working concentration solution (40-80mM), the 1M stock was directly diluted in cell culture media.

WST-1 Protocol

Materials for WST-1		
Product	**Vendor**	**Catalog Number**
WST-1 Reagent	Sigma/Roche	5015944001

1. Cells were seeded at 5,000 cells/cm^2 density in 96 well plates, leaving a few wells with media only for blanking.
2. After 24- 96 hours, WST-1 reagent was added to directly to cell culture medium at 1:10 concentration and mixed gently by pipetting, including
3. Plates were incubated for one hour at 37°C.
4. Plates were read at 420nm in a multiplate reader on absorbance mode.

Picogreen Protocol

Materials		
Product	**Vendor**	**Catalog Number**
Picogreen QuantIT Kit (Contains 20X TE Buffer, Lambda DNA Standard, and Picogreen Reagent	Invitrogen/ThermoFisher	P11496
Triton X-100	Sigma	X100-100ML

2D sample preparation for Picogreen

1. Media was aspirated from the well.
2. 1X TE Buffer was prepared with 0.02% Triton as lysis buffer.
3. For each well in a 48 well plate, 100uL 1X TE with 0.02% Triton was added and incubated for 10 minutes.
4. After 10 minutes, the resulting lysate containing DNA was used for Picogreen.

3D sample preparation for Picogreen

1. Media was gently aspirated from the well and the sponge.
2. 1X TE Buffer was prepared with 0.02% Triton for lysis buffer.
3. Each scaffold was removed and placed in an Eppendorf tube with 200uL lysis buffer.
4. Each scaffold was minced with small scissors.
5. The resulting lysate was used for Picogreen, taking care to only pipette liquid and not small pieces of scaffold.

Picogreen Protocol

1. A standard curve from 0-1000 ng/mL lambda phage DNA was prepared in TE buffer and placed in triplicate on each Picogreen plate. Black opaque plates were used for Picogreen.
2. 100µL of each sample in triplicate was added to the Picogreen plate.
3. Picogreen reagent was diluted 1:200 in TE buffer immediately before use.
4. 100µL of 1:200 diluted Picogreen Reagent was quickly added to each well of the plate using a multichannel pipette and incubated for 2-3 minutes in the dark.
5. Plates were immediately read at 485/538 nm using a fluorescence plate reader.
6. The lambda DNA standard curve was used to determine DNA concentration in samples.

Silk Scaffold Preparation Protocol

Materials for Silk Scaffold Preparation		
Product	**Vendor**	**Catalog Number**
Silk cocoons	Tajima Shoji	N/A
Lithium Bromide	Sigma	213225
Sodium Chloride	Sigma	S7653

1. *Bombyx mori* cocoons were chopped into roughly 2 cm squares and the inner worm was removed.
2. Cocoon pieces were then boiled for 30 minutes in 0.02M Na_2CO_3 and rinsed to remove sericin, leaving silk fibroin.
3. Fibroin was then solubilized in 9M LiBr before dialysis against water to obtain 6% weight/volume silk fibroin solution.
4. Twenty grams of 500-600μm size granular NaCl was added to 10mL silk fibroin solution in a petri dishes and incubated at room temperature for 24 hours.
5. Scaffolds were then soaked in water for two days with several water changes to remove the granular NaCl.
6. The resulting sponge was punched out with a 6mm diameter biopsy punch and scaffolds were trimmed to 2mm thickness.
7. Scaffolds were autoclaved before use in cell culture.

2D Migration and Proliferation Scratch Assay Protocol (Adapted from Liang et al., 2007)

1. hASCs were seeded at 15,000 cells per cm2 density in a 24 well plate and cultured for 24 hours.
2. The time lapse apparatus was attached to the Keyence microscope and equilibrated to 37 degrees.
3. After 24 hours, a P10 pipette tip was used to make a scratch across the center of each well. Care was taken to make the scratch as straight and consistent as possible.
4. The media was changed to remove scratched cells and to add drug (either 0.1μM ivermectin or 60mM potassium gluconate).
5. The 24 well plate was placed in the time lapse chamber.
6. A field of view was selected from each well to include the scratched area and a Z range was selected to account for microscope drift.
7. Brightfield images were taken every 30 minutes for 40 hours.
8. Best focus images were selected and used to make time lapse movies and to perform scratch area analysis.
9. The program CellProfiler (Carpenter et al., 2006) was used to analyze scratch assay data.

3D Migration and Proliferation Model Protocol

Materials for 3D Migration and Proliferation Assay		
Product	**Vendor**	**Catalog Number**
6mm diameter by 2mm thickness salt leached silk fibroin scaffolds	Kaplan Lab	N/A
Laminin	Sigma	L2020-1mg

1. Silk fibroin scaffolds (6mm diameter by 2mm thickness) were coated laminin in PBS for one hour at 37°C, then rinsed with ASC media.
2. Cells were seeded at 500,000 cells in 50µL volume and allowed to attach to scaffolds for one hour before 450µL additional media was added to the well. Scaffolds were incubated at 37°C in a humidified incubator with 5% CO_2 for 24 hours.
3. A third, empty scaffold was then abutted between the two seeded scaffolds after 48 hours and secured. Media was changed every 48 hours. After two to ten days, cell number was measured by Picogreen in both the outer and inner scaffolds.

Membrane Potential Measurement Protocols

Materials for Voltage Dye Staining		
Product	**Vendor**	**Catalog Number**
SS44 Di-Anionic	Akita Innovations	N/A
Di-8-ANEPPS	Sigma	D3167
DiSBAC2(3)	Sigma	K1018
DiBAC4(3)	Sigma	B438

SS44 (Di-Anionic) Staining Protocol

1. Cells were incubated in 200 nM SS44 (di-anionic) diluted in media for one hour at 37°C.
2. The 200nM SS44DA solution was gently aspirated and cells were gently washed with pre-warmed PBS.
3. PBS was aspirated and pre-warmed media containing 2 nM SS44DA was replaced.
4. Cells were imaged with the Cy5 filter.
5. Note: This protocol balanced diffusion of dye out of cells with background due to excess free dye for up to two hours. However, it may need to be further optimized for cell type or for longer length time lapse imaging.

Other Voltage Dye Staining Protocols

1. Cells were incubated with 0.475µM $DiBAC_4(3)$ for one hour, 10µM $DiSBAC_2(3)$ for one hour, or 2µM Di-8-ANEPPS (ThermoFisher) for 30 minutes in cell culture media at 37°C.
2. For Di-8-ANEPPS, cultures were then gently washed twice with PBS before imaging, while $DiBAC_4(3)$ and $DiSBAC_2(3)$ samples were imaged without washing.

Whole-Cell Patch Clamping Protocol

1. ASCs were seeded at 5,000 cells/cm2 in a 35mm dish and cultured with and without 0.1µM ivermectin for three hours to five days.
2. Immediately before patch clamp measurement, cells were trypsinized for 15 seconds to round cells without detaching them.
3. Cells were then allowed to recover at 37°C for five minutes before measurement. Media was then aspirated and replaced with extracellular solution.
4. For ivermectin-treated conditions, the extracellular solution also contained ivermectin.
5. Patch pipettes were filled with intracellular solution, then membrane potential was measured at room temperature using whole cell patch clamp in current clamp mode.